Cell Reports

Article

# Accumulation of branched-chain amino acids reprograms glucose metabolism in CD8$^+$ T cells with enhanced effector function and anti-tumor response

## Graphical abstract

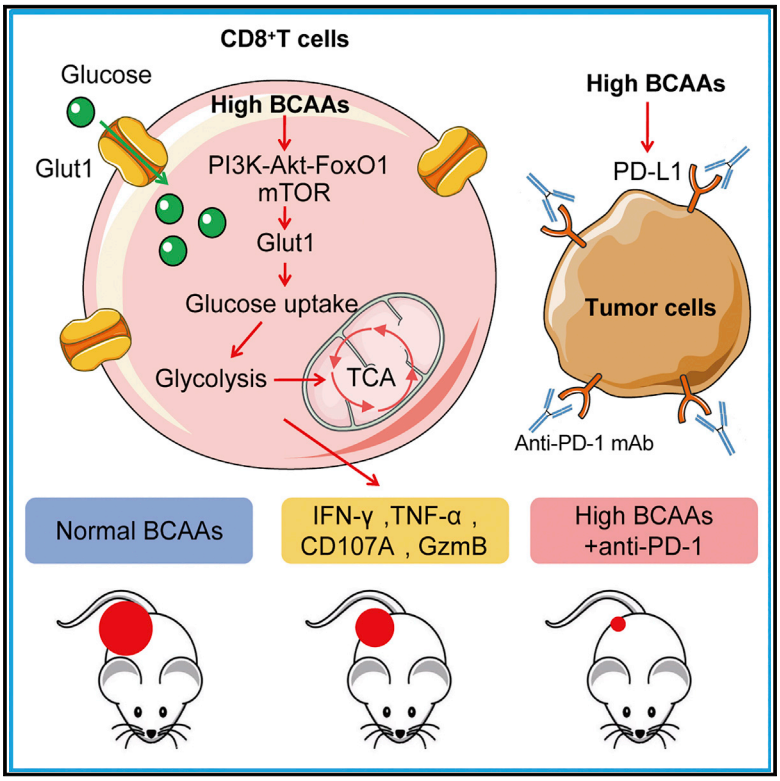


## Highlights

- CD8$^+$ T cells from *PP2Cm*$^{-/-}$ mice exhibit high BCAA content and enhanced functionality
- BCAA accumulation in CD8$^+$ T cells promotes Glut1 expression and glucose uptake
- BCAA supplementation magnifies CD8$^+$ T cell effector with altered glucose metabolism
- BCAAs synergize with anti-PD-1 regimen in anti-tumor immunity

## Authors

Cheng-cheng Yao, Rui-ming Sun, Yi Yang, ..., Shun Lu, Chen Yang, Ying Wang

## Correspondence

sun.haipeng@tmu.edu.cn (H.-p.S.), shunlu@sjtu.edu.cn (S.L.), cyang@cemps.ac.cn (C.Y.), ywangssmu@shsmu.edu.cn (Y.W.)

## In brief

Yao et al. report that BCAA accumulation in CD8$^+$ T cells upregulates Glut1 expression and increases glucose uptake, leading to reprogramming CD8$^+$ T cell metabolic features prone to anti-tumor immunity. BCAAs might become alternative supplementary components to increase the clinical efficacy of immune checkpoint inhibitors.

Yao et al., 2023, Cell Reports *42*, 112186
March 28, 2023 
https://doi.org/10.1016/j.celrep.2023.112186

CellPress

Cell Reports

CellPress
OPEN ACCESS

Article

# Accumulation of branched-chain amino acids reprograms glucose metabolism in CD8$^+$ T cells with enhanced effector function and anti-tumor response

Cheng-cheng Yao,[1,8] Rui-ming Sun,[1,8] Yi Yang,[3,8] Hai-yan Zhou,[2,4,8] Zhou-wenli Meng,[3] Rui Chi,[5] Li-liang Xia,[3] Ping Ji,[1] Ying-ying Chen,[1] Guo-qing Zhang,[6] Hai-peng Sun,[5,7,*] Shun Lu,[3,*] Chen Yang,[2,*] and Ying Wang[1,9,*]

[1]Shanghai Institute of Immunology, Department of Immunology and Microbiology, Key Laboratory of Cell Differentiation and Apoptosis of Chinese Ministry of Education, Shanghai Jiaotong University School of Medicine, Shanghai 200025, China
[2]CAS Key Laboratory of Synthetic Biology, CAS Center for Excellence in Molecular Plant Sciences, Chinese Academy of Sciences (CAS), Shanghai 200032, China
[3]Department of Shanghai Lung Cancer Center, Shanghai Chest Hospital, Shanghai Jiao Tong University, Shanghai 200030, China
[4]University of Chinese Academy of Sciences, Beijing 100049, China
[5]Department of Pathophysiology, Key Laboratory of Cell Differentiation and Apoptosis of Chinese Ministry of Education, Shanghai Jiao Tong University School of Medicine; Shanghai 200025, China
[6]Bio-Med Big Data Center, CAS Key Laboratory of Computational Biology, Shanghai Institute of Nutrition and Health, Chinese Academy of Science, Shanghai 200031, China
[7]NHC Key Laboratory of Hormones and Development, Center for Cardiovascular Diseases, The Province and Ministry Co-sponsored Collaborative Innovation Center for Medical Epigenetics, Chu Hsien-I Memorial Hospital & Tianjin Institute of Endocrinology, Tianjin Medical University, Tianjin 300134, China
[8]These authors contributed equally
[9]Lead contact
*Correspondence: sun.haipeng@tmu.edu.cn (H.-p.S.), shunlu@sjtu.edu.cn (S.L.), cyang@cemps.ac.cn (C.Y.), ywangssmu@shsmu.edu.cn (Y.W.)
https://doi.org/10.1016/j.celrep.2023.112186

## SUMMARY

Branched-chain amino acids (BCAAs) provide nutrient signals for cell survival and growth. How BCAAs affect CD8$^+$ T cell functions remains unexplored. Herein, we report that accumulation of BCAAs in CD8$^+$ T cells due to the impairment of BCAA degradation in *2C-type serine/threonine protein phosphatase* (*PP2Cm*)-deficient mice leads to hyper-activity of CD8$^+$ T cells and enhanced anti-tumor immunity. CD8$^+$ T cells from *PP2Cm*$^{-/-}$ mice upregulate glucose transporter Glut1 expression in a FoxO1-dependent manner with more glucose uptake, as well as increased glycolysis and oxidative phosphorylation. Moreover, BCAA supplementation recapitulates CD8$^+$ T cell hyper-functions and synergizes with anti-PD-1, in line with a better prognosis in NSCLC patients containing high BCAAs when receiving anti-PD-1 therapy. Our finding thus reveals that accumulation of BCAAs promotes effector function and anti-tumor immunity of CD8$^+$ T cells through reprogramming glucose metabolism, making BCAAs alternative supplementary components to increase the clinical efficacy of anti-PD-1 immunotherapy against tumors.

## INTRODUCTION

CD8$^+$ T cells are key components to exert immunity against infection and cancers through perforin/granzyme (Gzm)-mediated cytotoxicity and cytokine production including interferon (IFN)-$\gamma$ and tumor necrosis factor (TNF)-$\alpha$, etc. During the activation, proliferation, and differentiation processes, metabolic reprogramming in CD8$^+$ T cells is one of the key mechanisms to determine the destiny of immune responses.[1] When naive T cells are activated, they undergo a metabolic shift from oxidative phosphorylation (OXPHOS) to glycolysis for energy support and biomass production, while fatty acid oxidation is the main metabolic property for the maintenance of memory CD8$^+$ T cells.[2] Accordingly, intrinsic transcriptional,[3] post-translational,[4] epigenetic regulations,[5] as well as extrinsic nutrition factors,[6] are demonstrated to be extensively dedicated to metabolic modulation of CD8$^+$ T cell differentiation and function. In the tumor microenvironment (TME), metabolic fitness is also critical for anti-tumor immunity of local immune cells including CD8$^+$ T cells. To overcome the impairment of tumor-infiltrating T cells either due to the upregulation of co-inhibitors or by suppressive cytokines and surrounding cells etc.,[7] seeking metabolic strategies to preserve the functionality, especially in nutrient-limited TME is of great necessity for CD8$^+$ T cell-mediated anti-tumor immunity.

Branched-chain amino acids (BCAAs), including leucine, isoleucine, and valine, are essential amino acids obtained only from external diet supplementation.[8] They are building blocks

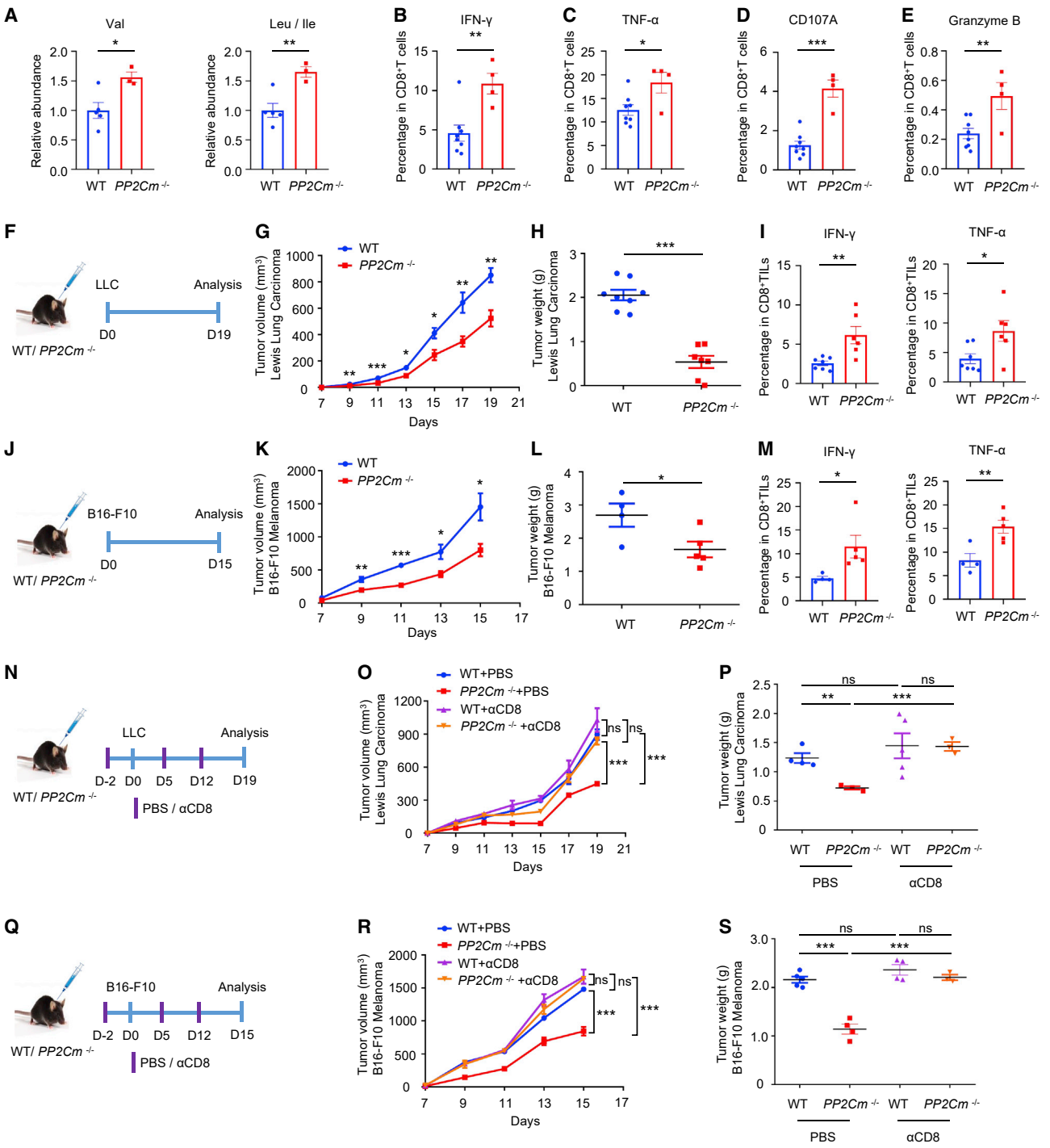


**Figure 1. *PP2Cm*$^{-/-}$ mice exhibit enhanced CD8$^+$ T cell functionality and anti-tumor immunity**

(A) Comparisons of intracellular Val (left) and Leu/Ile (right) levels in CD8$^+$ T cell from WT (n = 5) versus *PP2Cm*$^{-/-}$ (n = 3) mice.

(B–E) Percentages of IFN-γ$^+$ (B), TNF-α$^+$ (C), CD107A$^+$ (D), and GzmB$^+$ (E) CD8$^+$ T cells in the spleens of WT (n = 8) versus *PP2Cm*$^{-/-}$ (n = 4) mice.

(F) Experimental scheme.

(G and H) LLC tumor growth curves (G) and tumor weight at day 19 (H) in WT (n = 8) versus *PP2Cm*$^{-/-}$ mice (n = 7). Data from three independent experiments were pooled and presented.

(I) Percentages of IFN-γ$^+$ and TNF-α$^+$ CD8$^+$ T cells in LLC tumors from WT (n = 7) versus *PP2Cm*$^{-/-}$ mice (n = 6). Data from two independent experiments were pooled and presented.

(J) Experimental scheme.

*(legend continued on next page)*

for *de novo* synthesis and structural maintenance of endogenous proteins to maintain cell survival and cell growth.[9] BCAAs also serve as the precursors for biosynthesis of sterol and keto bodies.[10] They can further provide nutrient signals to regulate cellular metabolism and cell growth in a mammalian target of Rapamycin (mTOR)-dependent manner.[11] Being carbon and nitrogen sources, BCAA catabolism is initiated by the transamination of BCAAs into branched-chain a-keto acids (BCKAs) that are catalyzed by cytosolic or mitochondrial branched-chain aminotransferases (BCATs). BCKAs are then oxidized by branched-chain α-keto acid dehydrogenase (BCKD) complex and eventually degraded into the derivatives of coenzyme A (CoA), such as acetyl-CoA and succinyl-CoA.[12] In the BCAA catabolic pathway, BCKD is the bottleneck enzyme.[13] Its activity can be regulated by a mitochondrial 2C-type serine/threonine protein phosphatase (PP2Cm)[14] through directly binding to the BCKD complex for the activation.[15] Therefore, *PP2Cm* deficiency leads to elevated BCAAs in the periphery of *PP2Cm*-deficient mice.[16]

It has been widely reported that abnormal BCAA catabolism was associated with many diseases, including metabolic disorders,[17,18] heart diseases,[19] chronic liver diseases,[20] and certain malignances.[21] Investigations from heart failure models indicate that *PP2Cm* deficiency induces an increase in intracellular BCAA and BCKA levels, leading to mTOR activation, reactive oxygen species (ROS) production, and more susceptibility to calcium-induced permeability transition pore opening in cardiac myocytes.[22] Abnormal BCAA degradation is dedicated to cell proliferation in certain neoplasms such as glioma,[23] acute myeloid leukemia,[24] pancreatic duct adenocarcinoma (PDAC),[25] and hepatocellular carcinomas.[26] BCAAs are also capable of regulating immune responses. Accumulation of intracellular Leu activates the mTOR complex 1 (mTORC1) signaling pathway, which leads to the hyperactivation of $CD4^+$ T cells.[27] Our previous study showed that *BCAT1* was upregulated and *PP2Cm* was downregulated in human $CD8^+$ T cells following T cell receptor (TCR) triggered activation.[28] However, how the availability of BCAAs affects the differentiation and function of $CD8^+$ T cells with metabolic adaptation has not been addressed. A better understanding of how $CD8^+$ T cells responding to BCAA availability may aid in direct modulation of immune response against infection and cancers.

In this study, we reported that $CD8^+$ T cells from either $PP2Cm^{-/-}$ mice or BCAA-supplemented mice with accumulation of BCAAs exhibited hyper-activity with enhanced cytokine production and cytotoxicity as well as anti-tumor immunity. The underlying mechanisms of $CD8^+$ T cell hyper-activity were investigated together with synergistic roles of BCAAs in PD-1 blockade therapy, which might shed light on the potential of BCAAs as an alternative nutrient support in combination immunotherapy.

## RESULTS

### $PP2Cm^{-/-}$ mice exhibit enhanced $CD8^+$ T cell functionality and anti-tumor activity

Our previous studies reported that the expressions of key enzymes related to BCAA catabolism including *BCAT1* and *PP2Cm* have been altered upon TCR/CD28 stimulation in human $CD8^+$ T cells (Figure S1), implying the associations between BCAA catabolism and $CD8^+$ T cell activation. In $PP2Cm^{-/-}$ mice we have constructed previously,[13] there exhibited increased levels of intracellular (Figure 1A) and plasma (Figure S2A) BCAAs. No obvious defects in T cell development in the thymus were observed in $PP2Cm^{-/-}$mice (Figure S2B). However, there were slightly increased $CD8^+$ T cell proportions in the spleens when compared with wild-type (WT) littermates (Figure S2C). What is more, the proportions of IFN-γ, TNF-α, and granzyme B (GzmB) secreting $CD8^+$ T cells as well as $CD107A^+CD8^+$ T cells were exaggerated significantly in $PP2Cm^{-/-}$ mice (Figures 1B–1E), illustrating the enhancement of $CD8^+$ T cell effector functionality in $PP2Cm^{-/-}$ mice at steady states. Alternatively, the percentages of $CD4^+$ T cells, B cells, and natural killer (NK) cells (Figures S2D–S2F), the production of IFN-γ and TNF-α in $CD4^+$ T cells (Figures 2G and 2H) and $GzmB^+$ NK cells (Figure S2I) were mostly comparable between WT and $PP2Cm^{-/-}$ mice. We further examined anti-tumor responses in $PP2Cm^{-/-}$ mice by using syngeneic Lewis lung carcinoma (LLC)-grafted tumor models (Figure 1F). There was no difference in body weight between WT and $PP2Cm^{-/-}$ mice before and after being challenged with LLC cells (Figure S2J). $PP2Cm^{-/-}$ mice displayed remarkable retardation in tumor growth with less tumor weight when compared with WT mice (Figures 1G and 1H). Tumor-infiltrating $CD8^+$ T cells from $PP2Cm^{-/-}$ mice displayed increased IFN-γ and TNF-α production (Figure 1I), which was similar in the spleens from LLC-transplanted $PP2Cm^{-/-}$ mice (Figure S2K and S2L), as well as GzmB production (Figure S2M) when compared with those from WT littermates. Similarly, in B16-F10-grafted mice, tumor growth was slowed down (Figures 1J and 1K) and tumor weight was reduced (Figure 1L) while IFN-γ and TNF-α production in $CD8^+$ T cells were increased (Figure 1M) in $PP2Cm^{-/-}$ mice as compared with those in WT counterparts. To determine whether $CD8^+$ T cells are involved in tumor suppression in $PP2Cm^{-/-}$ mice, an anti-mouse CD8 monoclonal antibody (mAb) was used (Figure 1N) to deplete $CD8^+$ T cells in $PP2Cm^{-/-}$ and WT mice

(K and L) B16-F10 tumor growth curves (K) and tumor weight at day 15 (L) in WT (n = 4) versus $PP2Cm^{-/-}$ (n = 5) mice.
(M) Percentages of IFN-$\gamma^+$ and TNF-$\alpha^+$ $CD8^+$ T cells in B16-F10 tumors from WT (n = 4) versus $PP2Cm^{-/-}$ mice (n = 5).
(N) Experimental scheme.
(O and P) LLC tumor growth curves (O) and tumor weight (P) in WT + PBS (n = 4), $PP2Cm^{-/-}$ + PBS (n = 3), WT + anti-CD8 (n = 5) or $PP2Cm^{-/-}$ + anti-CD8 (n = 3) mice.
(Q) Experimental scheme.
(R and S) B16-F10 tumor growth curves (R) and tumor weight (S) in WT + PBS (n = 5), $PP2Cm^{-/-}$ + PBS (n = 4), WT + anti-CD8 (n = 4) or $PP2Cm^{-/-}$ + anti-CD8 (n = 3) mice. Data are presented as mean ± SEM. ns, non-significant; *p < 0.05, **p < 0.01, ***p < 0.001 by the Student's t test (A–S). Unless indicated, data are representative of two independent experiments.

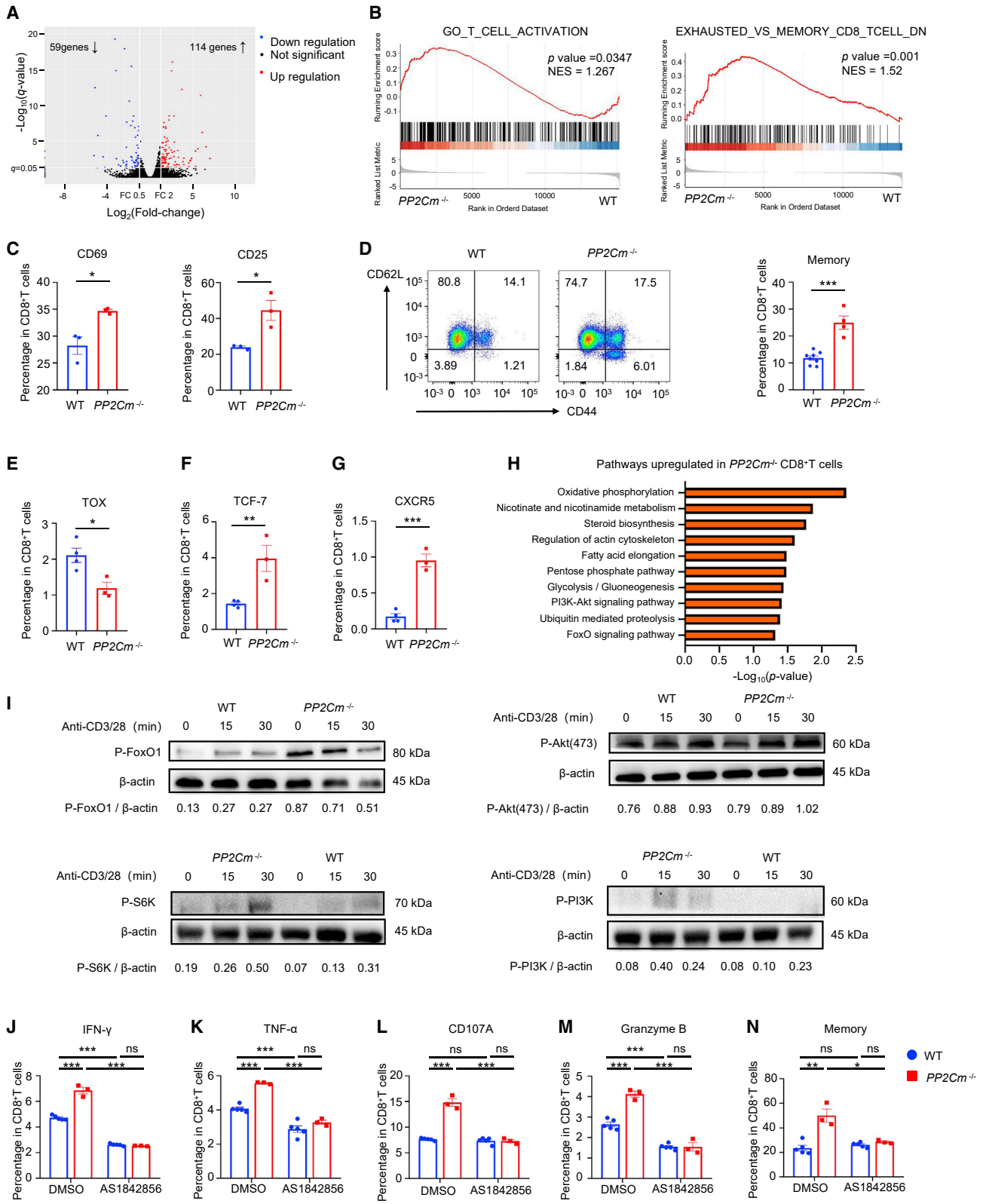


*(legend on next page)*

(Figure S2N). We found that the depletion of CD8$^+$ T cells abrogated the suppression of tumor growth in *PP2Cm*$^{-/-}$ mice with similar tumor growth and tumor weight to those in WT mice (Figures 1O and 1P). Similarly, tumor growth of B16-F10 cells in CD8$^+$ T cell-depleted *PP2Cm*$^{-/-}$ mice (Figure S2O) was also accelerated to similar levels in WT mice (Figures 1Q–1S). These results demonstrate that with the accumulation of BCAAs in *PP2Cm*$^{-/-}$ mice, CD8$^+$ T cells exhibit enhanced effector function and anti-tumor immunity.

### CD8$^+$ T cells from *PP2Cm*$^{-/-}$ mice possess activation and memory-like features with the activation of mTOR and PI3K-AKT-FoxO1 signaling axis

To further elucidate molecular signatures related to the enhancement of CD8$^+$ T cell functionality in *PP2Cm*$^{-/-}$ mice, we performed RNA sequencing (RNA-seq) transcriptome analysis on purified WT and *PP2Cm*$^{-/-}$ CD8$^+$ T cells upon anti-CD3/CD28 stimulation. There were 114 genes upregulated and 59 genes downregulated significantly in *PP2Cm*$^{-/-}$ CD8$^+$ T cells when compared with those from WT mice (Figure 2A). Gene set enrichment analysis (GSEA) plots showed the enrichment of activation (Figure 2B, left, false discovery rate [FDR]-adjusted p = 0.0347) and memory-like signatures (Figure 2B, right, FDR-adjusted p = 0.001). Consistently, higher proportions of CD69$^+$ and CD25$^+$CD8$^+$ T cells were present in the spleens from *PP2Cm*$^{-/-}$ mice when compared with WT littermates (Figure 2C), as well as more CD44$^+$CD8$^+$ memory T cells (Figure 2D). The expression of exhaustion-related transcription factor like TOX (Figure 2E) was reduced, whereas TCF-7 (Figure 2F) and CXCR5 (Figure 2G), the indicators for T cell stemness,[29] were upregulated in CD8$^+$ T cells from *PP2Cm*$^{-/-}$ mice. Similarly, tumor-infiltrating CD8$^+$ T cells from LLC-implanted *PP2Cm*$^{-/-}$ mice displayed more TCF-7 expression, and reduced PD-1, Tim-3, and TOX expressions as well (Figures S3A–S3D).

In addition, KEGG pathway enrichment analysis revealed that signaling pathways associated with cell survival and energetic metabolisms were significantly upregulated in *PP2Cm*$^{-/-}$ CD8$^+$ T cells after *in vitro* activation when compared with WT counterparts (Figure 2H). Since the mTOR pathway is widely reported to be regulated by BCAAs,[30] accumulation of BCAAs in *PP2Cm*$^{-/-}$ CD8$^+$ T cells also activated mTOR signaling demonstrated by increased phosphorylation of ribosomal protein S6, an indicator of mTORC1 activation, upon anti-CD3/CD28 stimulation (Figure 2I). PI3K-AKT-FoxO1 signaling pathway has been demonstrated previously to integrate metabolic and mitogenic signals in CD4$^+$ T cells,[31] which was also upregulated in *PP2Cm*$^{-/-}$ CD8$^+$ T cells based on RNA-seq data. We have observed that *PP2Cm*$^{-/-}$ CD8$^+$ T cells had elevated phosphorylation of PI3K, AKT$^{S473,}$ and FoxO1 when compared with WT counterparts (Figure 2I) as well. Moreover, the addition of AS1842856, a FoxO1 inhibitor,[32] led to a dramatic decrease in IFN-$\gamma$ and TNF-$\alpha$ production (Figures 2J and 2K), as well as the reduction of CD107A and GzmB (Figures 2L and 2M) in *PP2Cm*$^{-/-}$ CD8$^+$ T cells to similar levels of WT CD8$^+$ T cells. The percentages of CD44$^+$CD8$^+$ memory T cells also decreased to similar levels in WT counterparts (Figure 2N). Although the addition of Rapamycin, an mTORC1 inhibitor, led to a dramatic decrease in IFN-$\gamma$ and TNF-$\alpha$ as well as CD107A and GzmB in *PP2Cm*$^{-/-}$ CD8$^+$ T cells, they were still higher when compared with WT CD8$^+$ T cells (Figures S3E–S3H). These data indicate that CD8$^+$ T cells from *PP2Cm*$^{-/-}$ mice exhibit activation and memory-like features with hyper-activity of the PI3K-AKT-FoxO1 signaling axis, which is largely dedicated to enhanced immunoactivity.

### *PP2Cm*$^{-/-}$ CD8$^+$ T cells display highly activated glycolysis and OXPHOS

The transcriptomic analysis also showed that genes involved in glycolysis and OXPHOS were upregulated in *PP2Cm*$^{-/-}$ CD8$^+$ T cells (Figures 3A and 3B) with the enrichment of relevant gene signature plots from GSEA analysis (Figures S3I and S3J). Consistently, increased extracellular acidification rate (ECAR) occurred in *PP2Cm*$^{-/-}$ CD8$^+$ T cells with significantly elevated values of basal glycolysis, glycolytic capacity, and glycolytic reverse when compared with WT CD8$^+$ T cells (Figure 3C). *PP2Cm*$^{-/-}$ CD8$^+$ T cells also showed significantly higher mitochondrial oxygen consumption rate (OCR) with more mitochondrial spare respiratory capacity than WT CD8$^+$ T cells (Figure 3D). What is more, the expression level of glucose transporter 1 (Glut1), which is a key glucose importer on CD8$^+$ T cells,[33] was significantly increased in *PP2Cm*$^{-/-}$ CD8$^+$ T cells as compared with WT CD8$^+$ T cells both at the mRNA levels and protein levels demonstrated by RT-PCR and a small shift in flow cytometric analysis respectively (Figures 3E and 3F). Meanwhile, *PP2Cm*$^{-/-}$ CD8$^+$ T cells consumed more glucose than WT CD8$^+$ T cells upon anti-CD3/CD28 stimulation (Figure 3G), indicating an increase in glycolytic flux inside *PP2Cm*$^{-/-}$ CD8$^+$ T cells.

Therefore, we further performed a comparative metabolomic analysis on activated CD8$^+$ T cells from *PP2Cm*$^{-/-}$ versus WT mice using a liquid chromatograph-mass spectrometer (LC-MS) (Figure S4A). Not surprisingly, BCAA accumulation was detectable in *PP2Cm*$^{-/-}$ CD8$^+$ T cells. Furthermore, we found that the concentrations of intracellular intermediates

**Figure 2. *PP2Cm*$^{-/-}$ CD8$^+$ T cells possess gene signatures with activation and memory-like features and hyperactivation of mTOR-PI3K-AKT-FoxO1 signaling axis**

(A) Volcano plots indicating the alterations of gene expressing profiles in WT versus *PP2Cm*$^{-/-}$ CD8$^+$ T cells.

(B) GSEA analysis indicating the activation (left) and overlapping exhausted versus memory CD8$^+$ T cell down sites (right).

(C) Percentages of CD69$^+$ and CD25$^+$ CD8$^+$ T cells in the spleens of WT (n = 3) versus *PP2Cm*$^{-/-}$ (n = 3) mice.

(D) Representative flow plots (left) and quantifications (right) of the percentages of memory CD8$^+$ T cells in WT (n = 8) versus *PP2Cm*$^{-/-}$mice (n = 4).

(E–G) Percentages of TOX$^+$ (E), TCF-7$^+$ (F), CXCR5$^+$ (G) CD8$^+$ T cells in the spleens of WT (n = 4) versus *PP2Cm*$^{-/-}$ (n = 3) mice.

(H) Enrichment of KEGG pathways upregulated in CD8$^+$ T cells from *PP2Cm*$^{-/-}$ mice compared with WT counterparts.

(I) Immunoblotting of P-S6K, P-PI3K, P-AKT (473), and P-FoxO1 in WT and *PP2Cm*$^{-/-}$CD8$^+$ T cells upon anti-CD3/CD28 stimulation. The expression levels of target proteins were normalized with corresponding $\beta$-actin.

(J–N) Percentages of IFN-$\gamma^+$ (K), TNF-$\alpha^+$ (L), CD107A$^+$(M), GzmB$^+$ (N), and CD44$^+$ (O) CD8$^+$ T cells upon treatment with AS1842856 versus DMSO. Data are presented as mean ± SEM. *p < 0.05, **p < 0.01, ***p < 0.001 by the Student's t test (C–G, J–N). Data are representative of two independent experiments.

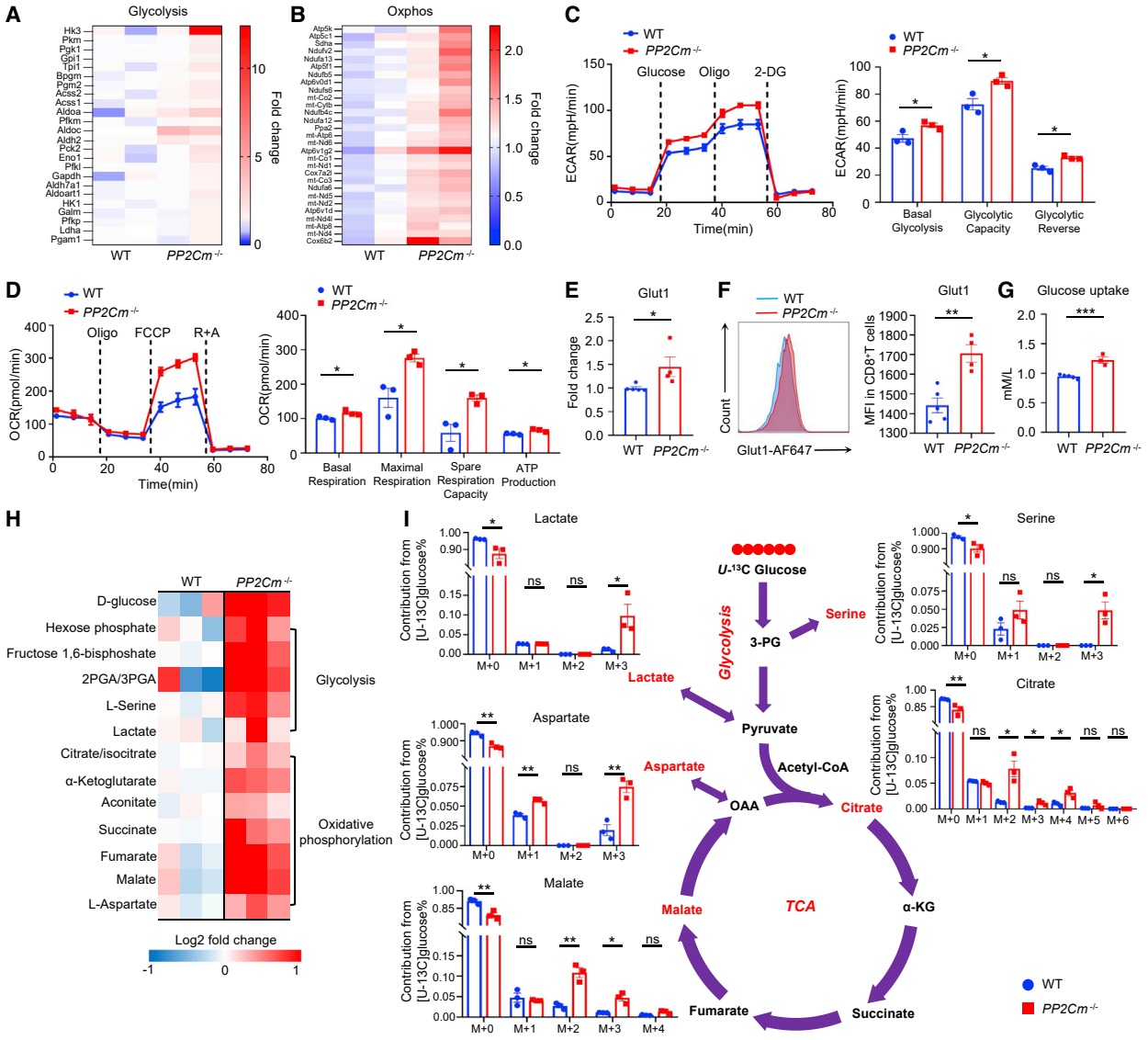


*(legend on next page)*

involved in glycolytic pathway including hexose-6-phosphates, fructose-1,6-bisphosphate (FBP), and 3-phosphoglycerate (3PGA) were increased in *PP2Cm*$^{-/-}$ CD8$^+$ T cells (Figure 3H). An accumulation of pyruvate was also detectable together with an elevated extracellular level of lactate in *PP2Cm*$^{-/-}$ CD8$^+$ T cells. In addition, we observed a significant increase in tricarboxylic acid (TCA) cycle intermediates including citrate, α-ketoglutarate (α-KG), succinate, fumarate, and malate in *PP2Cm*$^{-/-}$ CD8$^+$ T cells (Figure 3H). Amino acids like serine and aspartate that could be synthesized from glycolytic and TCA cycle intermediates were also accumulated in *PP2Cm*$^{-/-}$ CD8$^+$ T cells (Figure S4A). Moreover, the tracing experiments with uniformly labeled [*U*-$^{13}$C] glucose (Figure 3I) showed a notable increase in the fractions of glycolysis-derived serine and lactate, and TCA cycle-related citrate, aspartate, and malate in *PP2Cm*$^{-/-}$ CD8$^+$ T cells when compared with WT counterparts. When we added WZB117, a Glut1 inhibitor,[34] to CD8$^+$ T cells during anti-CD3/CD28 stimulation, the activities of glycolysis and OXPHOS were substantially suppressed in *PP2Cm*$^{-/-}$ CD8$^+$ T cells with dramatic decreases in relevant key intermediates (Figures S4B–S4J). When WZB117, 2-deoxyglucose (2-DG), and oligomycin (Oligo), which are the inhibitors of Glut1, glycolysis, and OXPHOS, respectively, were added during the activation of CD8$^+$ T cells, there resulted in an apparent reduction of *PP2Cm*$^{-/-}$ CD8$^+$ T cells expressing IFN-γ, TNF-α, CD107A, and GzmB to the base levels of WT CD8$^+$ T cells (Figures 3J–3M). Therefore, upregulation of glycolysis and OXPHOS initiated from Glut1 over-expression and more glucose uptake is dedicated to enhanced effector function of CD8$^+$ T cells in *PP2Cm*$^{-/-}$ mice.

## BCAA supplementation upregulates glycolysis and OXPHOS activity in CD8$^+$ T cells with functional enhancement

Aforementioned results from *PP2Cm*$^{-/-}$ mice strongly imply that accumulation of intracellular BCAAs promotes CD8$^+$ T cell functionality largely through modulating glucose metabolism. Whether external supplementation of BCAAs recapitulates *PP2Cm* deficiency mediated BCAA accumulation leading to the enhancement of CD8$^+$ T cell functions is further investigated. First, we stimulated the splenocytes from WT mice with anti-CD3/CD28 antibodies in the presence of gradient concentrations of BCAAs *in vitro*. We found that the percentages of IFN-γ and TNF-α producing CD8$^+$ T cells as well GzmB$^+$CD8$^+$ T cells increased significantly in a dose-dependent manner (Figures 4A–4C). The percentages of CD44$^+$CD8$^+$ T cells and the cytotoxicity of CD8$^+$ T cells to LLC cells *in vitro* were elevated at high BCAA concentrations as well (Figure S5A and S5B). Since PP2Cm is the key phosphatase to regulate the catabolism of BCAAs, we further used a PP2Cm inhibitor Sanguinarine chloride (SC) to analyze the roles of PP2Cm enzymatic activity in modulating CD8$^+$ T cell functionality. It was apparent that addition of SC led to the over-activation of CD8$^+$ T cells with increased percentages of IFN-γ$^+$, TNF-α$^+$, GzmB$^+$, and CD107A$^+$ CD8$^+$ T cells when compared with DMSO treatment. When BCAAs were free in the culture medium, the enhancement of CD8$^+$ T cell functionality was suppressed even with the addition of SC (Figures S5C–S5F). Moreover, the addition of BCAAs resulted in an increase in phospho-S6K and phospho-FoxO1 (Figure 4D) in CD8$^+$ T cells upon *in vitro* activation. When we fed the mice with extra BCAAs in water (Figure S5H), BCAA-supplemented mice (indicated as High BCAA) possessed higher levels of plasma BCAAs than non-supplemented mice (indicated as Normal BCAA) (Figures 4E and 4F). The abundance of total and memory CD8$^+$ T cells in the spleens from the High BCAA group was increased compared with those in the Normal BCAA group (Figures 4G and 4H), whereas the percentages of CD4$^+$ T cells, B cells, and NK cells were similar in both groups (Figure S5I). The expression of TCF-7 in CD8$^+$ T cells was also significantly upregulated in the High BCAA group when compared with the Normal BCAA group (Figure S5J). Similar to *PP2Cm*$^{-/-}$ mice, High BCAA group mice showed the increases in IFN–γ and TNF-α production by CD8$^+$ T cells (Figures 4I and 4J), and the proportions of CD107A$^+$ and GzmB$^+$ CD8$^+$ T cells (Figures 4K and 4L) as well as tumor-killing capacity of CD8$^+$ T cells (Figure S5K) as compared with Normal BCAA group mice. When we adoptively transferred CD8$^+$ T cells from normal and high BCAA-fed WT mice into *Rag1*$^{-/-}$ mice and detected LLC tumor growth *in vivo*, it was found that tumor volumes in *Rag1*$^{-/-}$ mice containing CD8$^+$ T cells from high BCAA-fed mice were smaller than those from normal BCAA-fed mice (Figure S5L). CD8$^+$ T cells from the High BCAA group also exhibited increased phospho-PI3K, phospho-S6K, phospho-AKT$^{S473}$, and phospho-FoxO1 (Figure S5M). Inhibition of FoxO1 activity diminished the increase in cytokine production (Figures S5N and S5O) and the cytotoxicity (Figures S5P and S5Q) in activated CD8$^+$

**Figure 3. *PP2Cm* deficiency promotes glycolysis and OXPHOS activities in CD8$^+$ T cells**

(A and B) Heatmaps showing relative expression of the genes involved in glycolysis and OXPHOS in CD8$^+$ T cells from WT (n = 2) versus *PP2Cm*$^{-/-}$ mice (n = 2).

(C) ECAR influxes of CD8$^+$ T cells from WT (n = 3) versus *PP2Cm*$^{-/-}$ mice (n = 3). Seahorse assay was performed with activated CD8$^+$ T cells.

(D) OCR influxes of CD8$^+$ T cells from WT (n = 3) versus *PP2Cm*$^{-/-}$ mice (n = 3).

(E and F) Detection of *Glut1* expression on CD8$^+$ T cells from WT (n = 5) and *PP2Cm*$^{-/-}$ (n = 4) mice by qPCR with fold changes (E) and by flow cytometry indicated by mean fluorescence intensity (MFI) (F).

(G) Glucose uptake by CD8$^+$ T cells (G) from WT (n = 5) versus *PP2Cm*$^{-/-}$(n = 4) mice. Glucose concentration in the supernatant was measured after anti-CD3/CD28 stimulation.

(H) Heatmap showing the ratio of the concentrations of intracellular glycolysis and TCA cycle intermediates in activated CD8$^+$ T cells from WT (n = 3) versus *PP2Cm*$^{-/-}$ (n = 3) mice.

(I) Mass isotopomer distribution (MID) of cellular metabolites in CD8$^+$ T cells upon anti-CD3/CD28 stimulation for 24 h. The incorporation of $^{13}$C atoms from glucose are denoted as M + n, where n is the number of $^{13}$C atoms and M means mass isotopomer.

(J–M) Percentages of IFN-γ$^+$ (J), TNF-α$^+$ (K), CD107A$^+$ (L), and GzmB$^+$ (M) CD8$^+$T cells upon treatment with PBS, 2-DG, and Oligomycin or DMSO versus WZB117. Data are presented as mean ± SEM. *p < 0.05, **p < 0.01, ***p < 0.001 by Student's t test (C–M). Data are representative of two independent experiments.

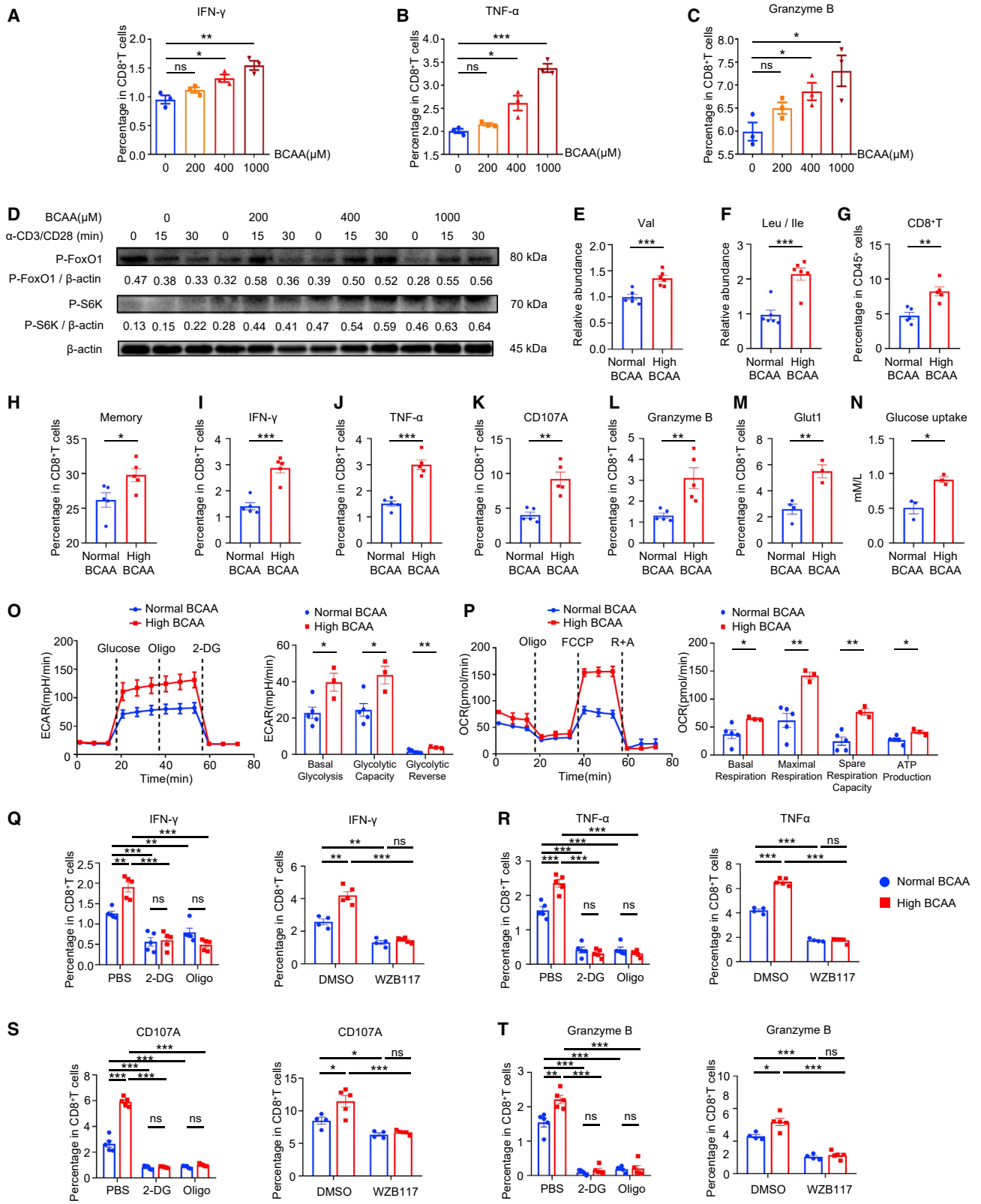


*(legend on next page)*

T cells from High BCAA group mice when compared with Normal BCAA group mice. These results demonstrate that BCAA supplementation promotes the activation and effector function of $CD8^+$ T cells both *in vitro* and *in vivo*.

Since Glut1 expression was upregulated on $CD8^+$ T cells from High BCAA group mice (Figure 4M) together with the increased capability of glucose uptake (Figure 4N), which was relying on FoxO1 activity (Figure S5R) as well as PP2Cm enzymatic activity (Figure S5G), we examined the metabolic consequence of BCAA supplementation. $CD8^+$ T cells from High BCAA group mice showed significantly increased ECAR (Figure 4O) and OCR (Figure 4P) influxes when compared with those from Normal BCAA group mice. Intracellular Val and Ile/Leu were accumulated and the concentrations of intracellular glycolytic and TCA cycle intermediates were increased in $CD8^+$ T cells from High BCAA group mice according to the metabolomic analysis (Figure S6A). Treatment of $CD8^+$ T cells from High BCAA group mice with WZB117, 2-DG, or Oligo reduced their cytokine production (Figures 4Q and 4R) and tumor-killing capacity (Figures 4S and 4T) to the base levels in Normal BCAA group mice. WZB117 treatment also downregulated the abundance of glycolysis and TCA cycle intermediates in $CD8^+$ T cells from High BCAA group mice (Figures S6B–S6F). In addition, WZB117 treatment also downregulated TCF-7 expression (Figure S6G) and upregulated Tim-3 and PD-1 (Figures S6H and S6I). Therefore, BCAA supplementation leads to the accumulation of BCAAs inside $CD8^+$ T cells with hyper-function through the upregulation of Glut1 and increased glycolysis and OXPHOS activities.

## BCAA supplementation synergizes with anti-PD-1 regimen in anti-tumor immunity

Given that accumulated intracellular BCAAs promote the activation and effector functions of $CD8^+$ T cells, we sought to determine whether BCAA supplementation could enhance anti-tumor efficacy either alone or with the combination of programmed cell death protein 1 (PD-1) blockade therapy in mice harboring LLC or B16-F10 tumors (Figure 5A). There was no dramatic difference in tumor growth and tumor weight of LLC and B16-F10 implanted tumors between High and Normal BCAA group mice (Figures 5B and 5C, blue and red). However, the addition of anti-PD-1 Ab significantly slowed down tumor growth with less tumor weight in High BCAA group mice (Figures 5B and 5C, orange lines and dots). When defining the properties of tumor-infiltrating $CD8^+$ T cells in High and Normal BCAA group mice with or without anti-PD-1 injection, we found that infiltrating $CD8^+$ T cells contained more IFN-$\gamma$ and TNF-$\alpha$ producing (Figures 5D and 5E), and CD107A and GzmB-positive proportions (Figures 5F and 5G) in LLC and B16-F10-grafted tumors (Figures S7A–S7D). Infiltrating $CD8^+$ T cells from High BCAAs + anti-PD-1 Ab-treated tumors exhibited the lowest expressions of TOX (Figure S7E) and the highest expressions of TCF-7 and CXCR5 (Figures S7F and S7G) among four groups. These results thus reveal that although high BCAA content alone does not suppress tumor growth, the addition of anti-PD-1 intervention is likely to trigger infiltrating $CD8^+$ T cells with more functional signatures, which in turn amplifies anti-tumoral response to restrain tumor growth.

Previous studies have reported the roles of BCAAs in tumorigenesis.[35] We also observed the effects of BCAAs in promoting the proliferation of LLC and B16-F10 *in vitro* in a dose-dependent manner significantly (Figure S7H). Interestingly, when coculturing WT splenocytes with LLC tumor cells *in vitro* at different concentrations of BCAAs, we found that the expression levels of PD-L1 on LLC cells were increased significantly at high BCAA concentrations (Figure 5H). In the *in vivo* models, PD-L1 expressions were also higher in LLC-implanted tumors from High BCAA group mice when compared with those from Normal BCAA group mice (Figure 5I). With the additional injection of anti-PD-1 Ab, there displayed downregulation of PD-L1 levels in tumor regions from High BCAA + anti-PD-1 group mice with more significance (Figure 5J). Since high BCAAs induced Glut1 expression on $CD8^+$ T cells leading to more glucose uptake (Figures 4M and 4N), we also compared Glut1 expressions on infiltrating $CD8^+$ T cells among four groups. It was found that LLC grafted tumors from High BCAA group mice displayed increased Glut1 expression on infiltrating $CD8^+$ T cells when compared with those from Normal BCAA group mice no matter with or without anti-PD-1 treatment (Figure 5K). Considering the sequential treatment of BCAAs (early) and anti-PD-1 Ab (late) in our experimental models, our data strongly imply that BCAA supplementation upregulates Glut1 expression on $CD8^+$ T cells, which in turn facilitates infiltrating $CD8^+$ T cells to uptake more glucose and synergize with anti-PD-1 in regional anti-tumor immunity.

## High BCAAs promote the activation of human $CD8^+$ T cells and are associated with improved clinical outcomes of anti-PD-1 therapy in non-small cell lung cancer

Our data from mouse models supported that BCAA accumulation either with intrinsic catabolism defect (*PP2Cm* deficiency) or external supplementation favored $CD8^+$ T cell hyper-functionality and synergized with anti-PD-1 therapy in anti-tumor

**Figure 4. BCAA supplementation upregulates glycolysis and OXPHOS activity in $CD8^+$ T cells with functional enhancement**

(A–C) Percentages of IFN-$\gamma^+$ (A), TNF-$\alpha^+$ (B) and $GzmB^+$ (C) $CD8^+$ T cells from WT mice (n = 3) treated with gradient BCAAs *in vitro*.

(D) Immunoblotting analysis of the indicated proteins in $CD8^+$ T cells from WT mice upon anti-CD3/28 stimulation with gradient BCAA concentrations *in vitro*.

(E and F) Levels of intracellular Val (left) and Leu/Ile (right) in mice fed with normal (n = 6) versus high BCAA (n = 6) water.

(G–L) Frequencies of total $CD8^+$ T cells (G) and percentages of $CD44^+$ (H), IFN-$\gamma^+$ (I), TNF-$\alpha^+$ (J), $CD107A^+$ (K) and $GzmB^+$ (L) $CD8^+$ T cells in the spleens from the mice fed with normal (n = 5) versus high BCAA (n = 5) water.

(M and N) Glut1 expression levels (M) and glucose uptake (N) in $CD8^+$ T cells from the mice fed with normal (n = 5) versus high BCAA (n = 5) water.

(O) ECAR influxes of $CD8^+$ T cells from the mice fed with normal (n = 3) versus high BCAA (n = 3) water. Seahorse assay was performed with activated $CD8^+$ T cells.

(P) OCR influxes of $CD8^+$ T cells from the mice fed with normal (n = 3) versus high BCAA (n = 3) water.

(Q–T) Percentages of IFN-$\gamma^+$ (Q), TNF-$\alpha^+$ (R), $CD107A^+$ (S), and $GzmB^+$ (T) $CD8^+$ T cells from the mice fed with normal (n = 3) versus high BCAA (n = 3) water upon treatment with PBS, 2-DG or Oligomycin or DMSO versus WZB117. Data are presented as mean ± SEM. ns, non-significant; *p < 0.05, **p < 0.01, ***p < 0.001 by Student's t test (A–C, E–T). Data are representative of two independent experiments.

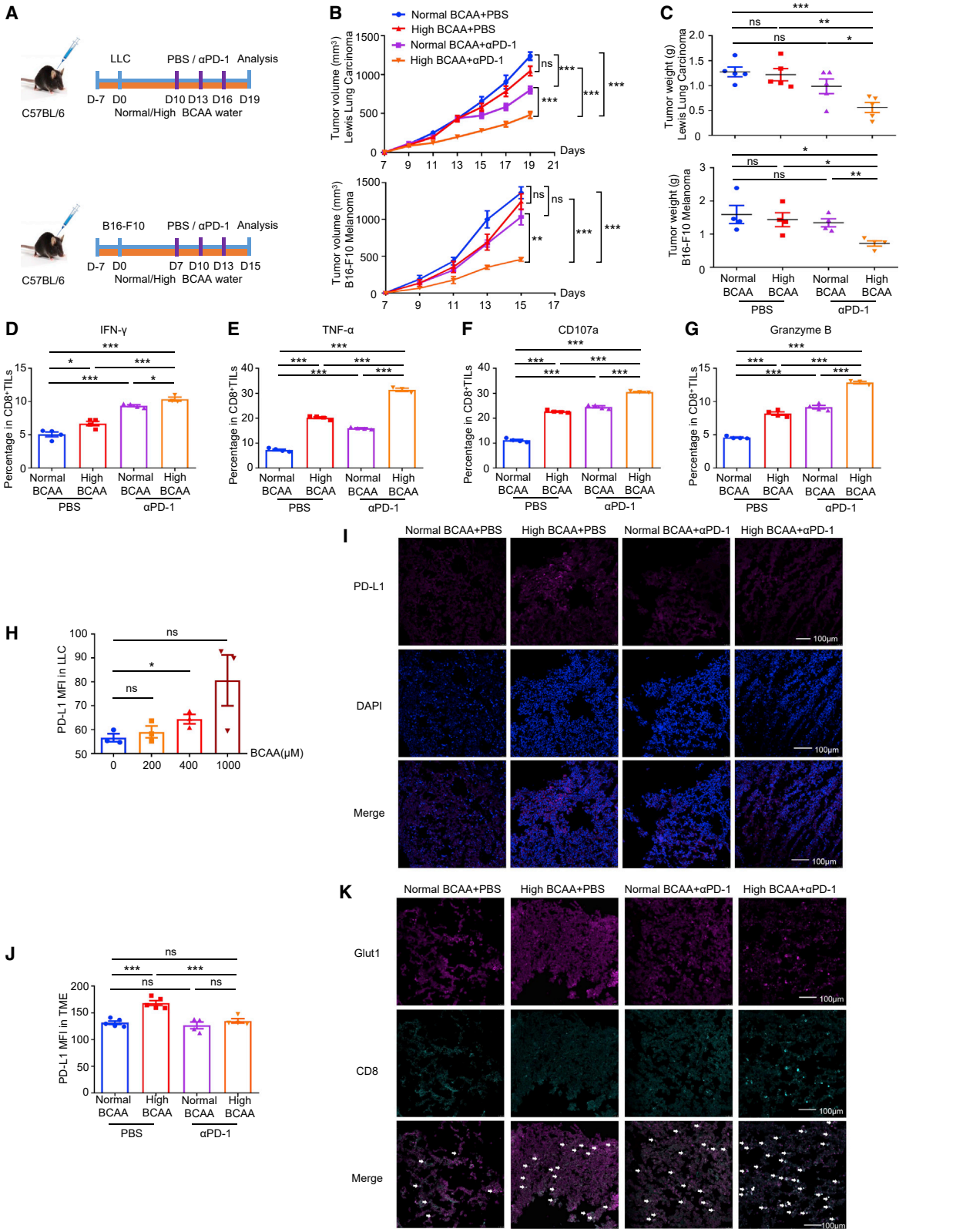


*(legend on next page)*

immunity. We further determined whether increased BCAAs also promoted the activation and function of human CD8$^+$ T cells. Peripheral blood mononuclear cells (PBMCs) were freshly isolated from healthy donors and activated by anti-CD3/CD28 *in vitro* in the presence of increasing concentrations of BCAAs. We found that BCAA supplementation increased the populations of CD8$^+$ T cells expressing TNF-$\alpha$ and GzmB (Figures 6A and 6B) together with the upregulation of Glut1 expression along with increased BCAA concentrations (Figure 6C).

To assess the clinical significance of our findings, we determined serum BCAA levels in 24 patients with advanced non-small cell lung cancer (NSCLC) (Table S1) receiving nivolumab (an anti-PD-1 therapeutic antibody) treatment. Among them, 10 patients being evaluated as a partial response or stable disease at the first evaluation time were classified as the responders, and 14 with disease progression were classified as the non-responders. We found that the responders had significantly higher levels of Val and Leu/Ile than the non-responders after the first infusion of nivolumab (Figure 6D). High levels of serum Val and Leu/Ile were associated with improved overall survival (Val: hazard ratio [HR] = 0.2350; 95% confidence interval [CI], 0.070–0.792; p = 0.0185; Leu/Ile: HR = 0.2338; 95% CI, 0.0690–0.788; p = 0.0179) (Figure 6E). The abundance of free Leu/Ile was positively correlated with serum IFN-$\gamma$ and the percentages of peripheral central memory CD8$^+$ T cells (Figure 6F) in our patient cohorts. Therefore, high BCAAs also promote human CD8$^+$ T cell functionality and might be favorable to improve anti-PD-1 treatment in clinic.

## DISCUSSION

In the present study, we have demonstrated that accumulation of BCAAs either due to the impairment of BCAA catabolism with *PP2Cm* deficiency or through diet supplementation could induce CD8$^+$ T cell hyper-functionality largely through the upregulation of Glut1 and remodeling intracellular metabolic activity. Previous studies reported that the lack of dietary BCAAs impaired antibody production and the generation of cytotoxic T cells in response to *Salmonella typhimurium*.[36] On the contrary high BCAAs promote oxidative stress and inflammation of human PBMCs through mTORC1 activation.[37] In our study, BCAA accumulation became a triggering factor for hyper-functionality of CD8$^+$ T cells upon TCR/CD28 stimulation. When *PP2Cm*$^{-/-}$ mice were activated in low BCAA culture medium, the percentages of IFN-$\gamma^+$, TNF-$\alpha^+$, GzmB$^+$, and CD107A$^+$ CD8$^+$ T cells were downregulated to the similar levels in WT mice (Figures S2P–2S). The increased metabolism and functionality were attenuated as well (Figures S2T–S2Z). These results further support the requirement of high BCAAs in improving T cell functionality. What is more, Glut1 expression as well as glucose uptake are augmented, which largely contributes to the enhanced ECAR and OCR influxes in CD8$^+$ T cells from two BCAA-accumulated mouse models. It has been reported previously that BCAAs were able to regulate the expression of glucose transporter and glucose uptake in skeletal muscle.[38] Glut1 expression on CD8$^+$ T cells can also be triggered by TCR/CD28 stimulation and modulated by multiplex factors.[39] Since glucose is the primary energy resource for T cell activation, clonal expansion, and effector function,[40] upregulation of Glut1 and subsequent glucose uptake by CD8$^+$T cells under high BCAA content will favor the activation and maintenance of effector function in CD8$^+$ T cells as well as the suppression of exhaustion (Figures S6G–S6I). Moreover, results from both gene signature profiles and metabolomic analyses on *PP2Cm*$^{-/-}$ CD8$^+$ T cells reveal the reprogramming of glucose metabolism in CD8$^+$ T cells (Figure S4). In fact, high activity of both glycolysis and OXPHOS in CD8$^+$ T cells was also reported previously in *sirt2*$^{-/-}$ mice where *sirt2* deficiency provoked hyper-acetylation of multiple metabolic enzymes and amplification of their activities.[40] Herein we have also observed the upregulation of multiplex genes related to energy metabolism, supporting the roles of intrinsic high BCAA content in promoting gene expression through PI3K-AKT-Foxo1 signaling pathways. Interestingly, we did not enrich fatty acid metabolism-related pathway in *PP2Cm*$^{-/-}$ CD8$^+$ T cells (Figures S3K, p = 0.6712) with no difference in expression levels of relevant genes between WT and *PP2Cm*$^{-/-}$ CD8$^+$ T cells including *Cpt1a*, *ACAA2*, *ECHS1*, *ACSS1,* and *ACSS2* (Figures S3L–S3P). This might be because high BCAAs are more likely to serve as nutrient signal molecules to activate mTOR and other signaling pathways, and integrate multiple metabolic pathways to maintain memory-like phenotypes of CD8$^+$ T cells. Glut1 upregulation is one of the outcomes of accumulated BCAAs-triggered gene transcription, which in turn exaggerates glucose consumption and downstream metabolism to fulfill the requirement for the hyper-activity of CD8$^+$ T cells.

The fact that upregulation of Glut1 and increased glucose uptake dedicate to enhanced CD8$^+$ T cell functionality in high BCAA content might be more significant when CD8$^+$ T cells are infiltrating into tumor regions. The TME can be considered as a

**Figure 5. BCAA supplementation synergizes with anti-PD-1 regimen in anti-tumor immunity**

(A) Experimental scheme.

(B and C) Tumor growth (B) and tumor weight (C) of LLC (upper, n = 5 in each group) and B16-F10 (down, n = 4 for each group) transplanted tumors in the mice fed with normal versus high BCAA water with or without anti-PD1 antibody.

(D–G) Percentages of IFN-$\gamma^+$ (D), TNF-$\alpha^+$ (E), CD107A$^+$ (F), and GzmB$^+$ (G) CD8$^+$ T cells in LLC grafted tumors (n = 4 mice in each group) from the mice fed with normal or high BCAA water with or without anti-PD1 antibody.

(H) MFI values of PD-L1 on LLC cells after coculturing with WT CD8$^+$ T cells after anti-CD3/CD28 stimulation in gradient BCAA concentrations *in vitro*.

(I and J) Immunofluorescence staining (I) and MFI values (J) of PD-L1 in LLC grafted tumors from the mice fed with normal versus high BCAA water with or without anti-PD1 antibody (n = 5 in PBS group, n = 4 in anti-PD-1 group). Purple (Cy3) indicates the PD-L1. Blue (DAPI) indicates the nucleus. Scale bar, 100 $\mu$m (×200).

(K) Immunofluorescence staining of CD8 and Glut1 in LLC grafted tumors from the mice fed with normal versus high BCAA water with or without anti-PD1 antibody. Green (FITC) indicates CD8 and purple (Cy3) indicates Glut1. Blue (DAPI) indicates the nucleus. White arrows show co-location of CD8 and Glut1. Scale bar, 100 $\mu$m (×200). Data are presented as mean ± SEM. ns, non-significant; *p < 0.05, **p < 0.01, ***p < 0.001 by Student's t test. Data are representative of two independent experiments.

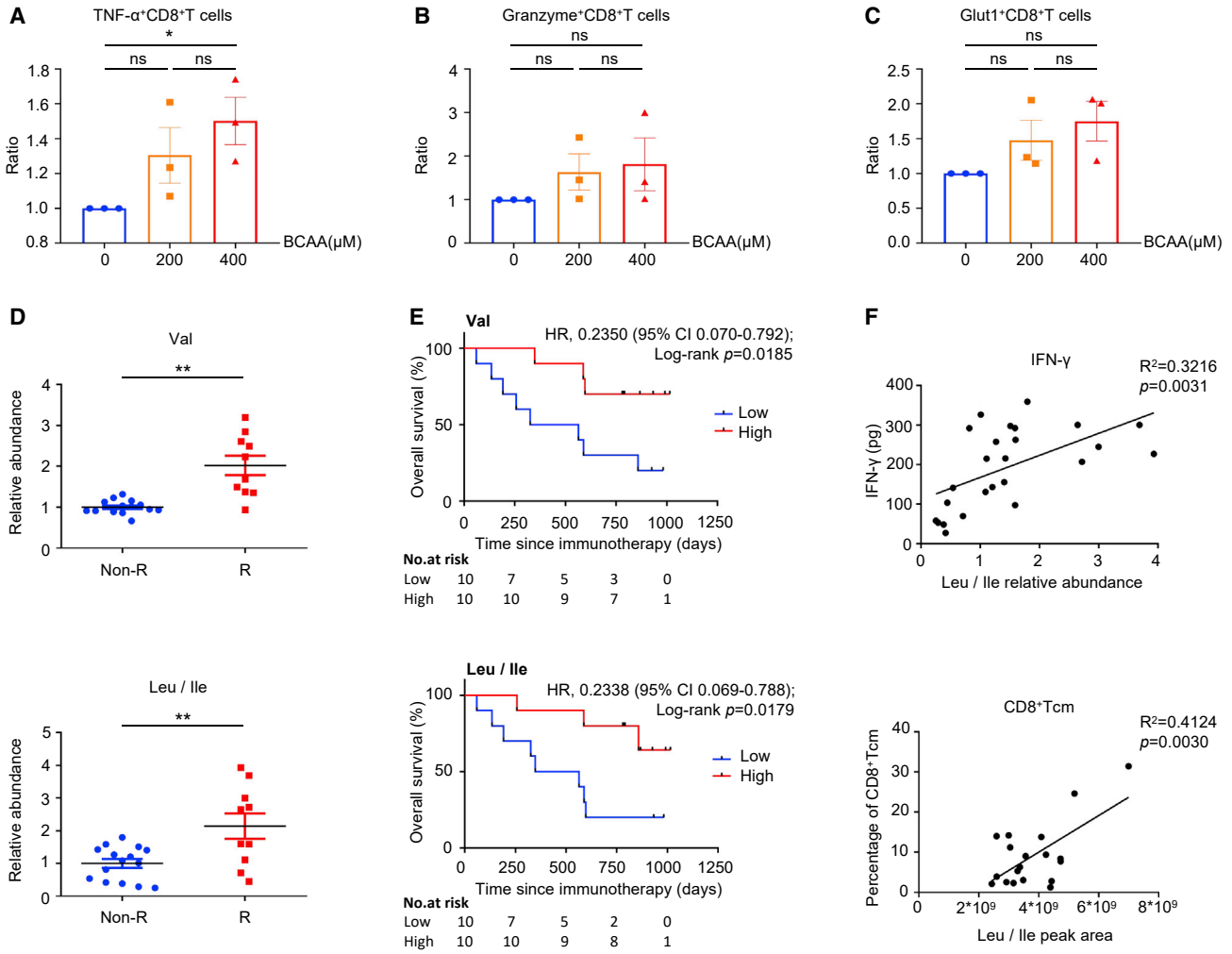


**Figure 6. High BCAAs promote human CD8⁺ T cell functionality and are associated with a better prognosis of anti-PD-1 immunotherapy in non-small cell lung cancer**

(A–C) Percentages of TNF-$\alpha^+$ (A), GzmB$^+$ (B), and Glut1$^+$ (C) CD8$^+$ T cells in PBMCs from healthy donors treated with gradient BCAA concentrations. Samples are normalized to BCAA free group.

(D) Val (upper) and Leu/Ile (lower) levels in the plasma of the responder versus the non-responder NSCLC patients.

(E) Kaplan-Meier (K-M) plots of overall survival (OS) with plasma Val (upper) and Leu/Ile (lower) of NSCLC patients after receiving nivolumab treatment.

(F) Spearman correlations of plasma Leu/Ile abundance with peripheral IFN-$\gamma$ levels (upper) and the percentages of peripheral central memory CD8$^+$ T cells (lower). Data are presented as mean ± SEM; **p < 0.01 by Student's t test (A–D). Survival curves for the PFS were estimated by using the Kaplan-Meier method (the log rank test). The Spearman correlation test was applied to define the associations between BCAA concentrations and immune parameters.

unique metabolic niche that can reshape biological properties of tumor cells, immune cells, and stromal cells inside.[41] A hallmark feature of tumor cell metabolism is increased nutrient consumption to meet energetic, anabolic, and pro-survival demands.[42] Tumor cells consume massive nutrition in priority for their proliferation leading to the generation of hypoxia, hypoglycemic, and acidic microenvironment, which makes local metabolic landscapes in ways that inhibit anti-tumor immunity.[43] To some extent, tumor cells in the TME establish a metabolic barrier for intratumoral CD8$^+$ T cells to exert normal anti-tumor immunity.[44] Based on our results, accumulation of BCAAs either due to *PP2Cm* knockdown or through external supplementation endows CD8$^+$ T cells with the capacity to increase the uptake of glucose through upregulation of Glut1 expression, which can largely promote T cell effector function in the TME. In the TME, this feature will be of more significance in facilitating CD8$^+$ T cells to compete with tumor cells for the utility of glucose, which in turn exaggerates energetic metabolism for the functional requirement. This pattern is mirrored by tumor-infiltrating CD8$^+$ T cells from BCAA-supplemented mice, indicating that metabolically stressed CD8$^+$ T cells inside tumors under a normal diet might be relieved by BCAA supplementation with the activation of Glut1-mediated glucose competition (Figure 5K).

Our study also provides new evidence on dietary perturbations for combination immunotherapy in tumor control. Previous

investigations demonstrated the beneficial roles of the diet on anti-tumor immunity. For instance, supplementations with inosine,[45] acetate,[46] or polyunsaturated fatty acids[47] under certain circumstances increase anti-tumor immunity. In this study we could not ignore the effects of BCAAs on tumor cells during BCAA supplementation. BCAAs are critical to providing carbon and nitrogen for macromolecule synthesis for tumor growth.[48] Several studies have reported tumorigenesis effects of BCAA metabolism on tumor cells. In our *in vivo* study, tumor growth was comparable with or without BCAA supplementation. Although we have also observed that BCAAs promoted tumor cell proliferation *in vitro* (Figure S7H), high BCAAs are able to increase $CD8^+$ T cell functionality, which in turn restrains tumor growth *in vivo*. We deduce that an extra BCAA diet may amplify the metabolic tug of war in tumors with more effects on the augmentation of local $CD8^+$ T cell functionality through the upregulation of glucose transporters. The addition of high BCAAs not only upregulates PD-L1 expression on tumor cells both *in vitro* and *in vivo* (Figures 5H–5J), but also enhances $CD8^+$ T cell functionality, which coordinates to favor clinical efficacy of immune checkpoint inhibitor (ICI) treatment. This is pretty well matched with clinical observations that high BCAA levels were favorable for anti-PD-1 reagent treatment. These correlation results together with BCAA supplementation experiments in the mice suggest that high BCAA-mediated metabolic adaptation of tumor-infiltrating $CD8^+$ T cells might be one of the key switches to increased anti-tumor immunity, which needs to be functionally confirmed in the future.

In summary, we report that accumulation of BCAAs induces metabolic rewiring of $CD8^+$ T cells, which in turn enhances their effector function and anti-tumor immunity. High BCAAs also work in synergy with PD-1 blockade in immunotherapy. With the help of extra BCAAs, metabolic reprogramming initiated from increased glucose uptake facilitates $CD8^+$ T cells with more glucose availability to compete with tumor cells in the TME and overcome the potential energy shortage, which fulfills enhanced anti-tumor immune responses locally. Since metabolic states of immune cells and tumor cells as well as other stroma cells within the tumors are coupled, our findings also provide new ways to remodel metabolic reciprocity in intratumoral immune cell populations for tumor control through BCAA supplementation. Once we understand more extensively the effects of BCAA supplementation on the interplay between systemic metabolism and the changes in the TME as well as the effects on the metabolisms of tumor and immune cells, nutrient manipulation with BCAA supplementation might be introduced as a potential combination therapy with ICIs in clinic.

### Limitations of the study

In this study, we have proposed that the accumulation of BCAAs reprogrammed glucose metabolism of tumor-infiltrating $CD8^+$ T cells, which was dedicated to enhanced anti-tumor immunity through Glut1 hyper-expression. It will be more evident if we could define the metabolic property of tumor infiltrating $CD8^+$ T cells as well as tumor cells in the TME to elucidate the roles of nutrition competition in anti-tumor immunity. Since BCAAs have been included in nutrient supply in clinic, we did not validate synergistic roles of BCAAs with anti-PD-1 regimen in clinic, which could provide clinical evidence on BCAAs for a better prognosis of advanced NSCLC patients receiving ICI treatment.

## STAR★METHODS

Detailed methods are provided in the online version of this paper and include the following:

- KEY RESOURCES TABLE
- RESOURCE AVAILABILITY
  - Lead contact
  - Materials availability
  - Data and code availability
- EXPERIMENTAL MODEL AND SUBJECT DETAILS
  - Human subjects
  - Mice
  - Cells lines
- METHOD DETAILS
  - Mouse tumor models
  - *In vivo* anti-PD-1 treatment
  - *In vivo* high or low BCAA-fed mouse model
  - *In vivo* T cell depletion
  - Preparation of mouse tumor infiltrating lymphocytes
  - Isolation of mouse $CD8^+$ T cells and *in vitro* stimulation
  - Preparation of human $CD8^+$ T cells and *in vitro* stimulation
  - Flow cytometry
  - Cell proliferation assay
  - RNA-sequencing analysis
  - Enrichment analysis
  - Western blot assay
  - Immunofluorescence analysis
  - Lactate dehydrogenase (LDH) release assay
  - Extracellular flux analysis
  - Detection of glucose consumption and lactate production
  - Metabolomic analysis
  - Luminex assay
  - RT-PCR
- QUANTIFICATION AND STATISTICAL ANALYSIS

## SUPPLEMENTAL INFORMATION

Supplemental information can be found online at https://doi.org/10.1016/j.celrep.2023.112186.

## ACKNOWLEDGMENTS

This study was supported by grants from the National Natural Science Foundation of China (81802264, 82073152, 82030045), the National Key R&D Program of China (2016YFC1303300), Science and Technology Innovation Program of Shanghai Municipal Government (19411950500, 20JC1417500), Shanghai Collaborative Innovation Center for Translational Medicine (TM202112), Talent Training Program of Shanghai Chest Hospital (2019), and Incubation Project Plan for Research in Shanghai Chest Hospital (2019YNJCM07). We appreciate Prof Guo-ping Zhao from the Key Lab of Computational Biology Shanghai Institutes for Biological Sciences, Chinese Academy of Sciences, to give us instructions and discussion on this project. We also appreciate the Core Facility of Basic Medical Sciences in Shanghai JiaoTong University School of Medicine for their technical support.

## AUTHOR CONTRIBUTIONS

Y.W., S.L., and H.P.S. initiated the study. Y.W. and C.C.Y. designed the project and directed the research; C.C.Y., R.M.S., and R.C. performed most of the experiment. H.Y.Z. and C.Y. performed the metabolic experiment and data analysis. S.L., Y.Y., W.L.M.Z., and L.L.X. were responsible for sample collection and data analysis. Y.W., C.C.Y., R.M.S., H.P.S., C.Y., and S.L. analyzed the data and drafted the manuscript. All authors contributed to the manuscript preparation.

## DECLARATION OF INTERESTS

The authors declare no competing interest.

Received: May 22, 2022
Revised: January 5, 2023
Accepted: February 14, 2023

## REFERENCES

1. Guo, Y., Xie, Y.Q., Gao, M., Zhao, Y., Franco, F., Wenes, M., Siddiqui, I., Bevilacqua, A., Wang, H., Yang, H., et al. (2021). Metabolic reprogramming of terminally exhausted CD8(+) T cells by IL-10 enhances anti-tumor immunity. Nat. Immunol. *22*, 746–756. https://doi.org/10.1038/s41590-021-00940-2.
2. Raud, B., McGuire, P.J., Jones, R.G., Sparwasser, T., and Berod, L. (2018). Fatty acid metabolism in CD8(+) T cell memory: challenging current concepts. Immunol. Rev. *283*, 213–231. https://doi.org/10.1111/imr.12655.
3. Lu, H., Liu, F., Li, Y., Wang, J., Ma, M., Gao, J., Wang, X., Shen, Z., and Wu, D. (2021). Chromatin accessibility of CD8 T cell differentiation and metabolic regulation. Cell Biol. Toxicol. *37*, 367–378. https://doi.org/10.1007/s10565-020-09546-0.
4. Russ, B.E., Olshansky, M., Li, J., Nguyen, M.L.T., Gearing, L.J., Nguyen, T.H.O., Olson, M.R., McQuilton, H.A., Nüssing, S., Khoury, G., et al. (2017). Regulation of H3K4me3 at transcriptional enhancers characterizes acquisition of virus-specific CD8(+) T cell-lineage-specific function. Cell Rep. *21*, 3624–3636. https://doi.org/10.1016/j.celrep.2017.11.097.
5. Franco, F., Jaccard, A., Romero, P., Yu, Y.R., and Ho, P.C. (2020). Metabolic and epigenetic regulation of T-cell exhaustion. Nat. Metab. *2*, 1001–1012. https://doi.org/10.1038/s42255-020-00280-9.
6. Papavassiliou, A.G., and Musti, A.M. (2020). The Multifaceted Output of c-Jun biological activity: focus at the junction of CD8 T cell activation and exhaustion. Cells *9*. https://doi.org/10.3390/cells9112470.
7. Lutsiak, M.E.C., Tagaya, Y., Adams, A.J., Schlom, J., and Sabzevari, H. (2008). Tumor-induced impairment of TCR signaling results in compromised functionality of tumor-infiltrating regulatory T cells. J. Immunol. *180*, 5871–5881. https://doi.org/10.4049/jimmunol.180.9.5871.
8. Yamamoto, K., Tsuchisaka, A., and Yukawa, H. (2017). Branched-chain amino acids. Adv. Biochem. Eng. Biotechnol. *159*, 103–128. https://doi.org/10.1007/10_2016_28.
9. Mero, A. (1999). Leucine supplementation and intensive training. Sports Med. *27*, 347–358. https://doi.org/10.2165/00007256-199927060-00001.
10. Cole, J.T., Sweatt, A.J., and Hutson, S.M. (2012). Expression of mitochondrial branched-chain aminotransferase and α-keto-acid dehydrogenase in rat brain: implications for neurotransmitter metabolism. Front. Neuroanat. *6*, 18. https://doi.org/10.3389/fnana.2012.00018.
11. Gu, Z., Liu, Y., Cai, F., Patrick, M., Zmajkovic, J., Cao, H., Zhang, Y., Tasdogan, A., Chen, M., Qi, L., et al. (2019). Loss of EZH2 Reprograms BCAA metabolism to drive leukemic transformation. Cancer Discov. *9*, 1228–1247. https://doi.org/10.1158/2159-8290.Cd-19-0152.
12. Brosnan, J.T., and Brosnan, M.E. (2006). Branched-chain amino acids: enzyme and substrate regulation. J. Nutr. *136*, 207s–211s. https://doi.org/10.1093/jn/136.1.207S.
13. Lu, G., Sun, H., She, P., Youn, J.Y., Warburton, S., Ping, P., Vondriska, T.M., Cai, H., Lynch, C.J., and Wang, Y. (2009). Protein phosphatase 2Cm is a critical regulator of branched-chain amino acid catabolism in mice and cultured cells. J. Clin. Invest. *119*, 1678–1687. https://doi.org/10.1172/jci38151.
14. Lian, K., Du, C., Liu, Y., Zhu, D., Yan, W., Zhang, H., Hong, Z., Liu, P., Zhang, L., Pei, H., et al. (2015). Impaired adiponectin signaling contributes to disturbed catabolism of branched-chain amino acids in diabetic mice. Diabetes *64*, 49–59. https://doi.org/10.2337/db14-0312.
15. Miller, R.H., and Harper, A.E. (1988). Regulation of valine and alpha-ketoisocaproate metabolism in rat kidney mitochondria. Am. J. Physiol. *255*, E475–E481. https://doi.org/10.1152/ajpendo.1988.255.4.E475.
16. Wang, J., Liu, Y., Lian, K., Shentu, X., Fang, J., Shao, J., Chen, M., Wang, Y., Zhou, M., and Sun, H. (2019). BCAA catabolic defect alters glucose metabolism in lean mice. Front. Physiol. *10*, 1140. https://doi.org/10.3389/fphys.2019.01140.
17. Lee, J., Vijayakumar, A., White, P.J., Xu, Y., Ilkayeva, O., Lynch, C.J., Newgard, C.B., and Kahn, B.B. (2021). BCAA supplementation in mice with diet-induced Obesity Alters the Metabolome without impairing glucose Homeostasis. Endocrinology *162*, bqab062. https://doi.org/10.1210/endocr/bqab062.
18. Lynch, C.J., and Adams, S.H. (2014). Branched-chain amino acids in metabolic signalling and insulin resistance. Nat. Rev. Endocrinol. *10*, 723–736. https://doi.org/10.1038/nrendo.2014.171.
19. Nie, C., He, T., Zhang, W., Zhang, G., and Ma, X. (2018). Branched chain amino acids: beyond nutrition metabolism. Int. J. Mol. Sci. *19*, 954. https://doi.org/10.3390/ijms19040954.
20. Katayama, K. (2020). Zinc and protein metabolism in chronic liver diseases. Nutr. Res. *74*, 1–9. https://doi.org/10.1016/j.nutres.2019.11.009.
21. Zhu, Z., Achreja, A., Meurs, N., Animasahun, O., Owen, S., Mittal, A., Parikh, P., Lo, T.W., Franco-Barraza, J., Shi, J., et al. (2020). Tumour-reprogrammed stromal BCAT1 fuels branched-chain ketoacid dependency in stromal-rich PDAC tumours. Nat. Metab. *2*, 775–792. https://doi.org/10.1038/s42255-020-0226-5.
22. Huang, Y., Zhou, M., Sun, H., and Wang, Y. (2011). Branched-chain amino acid metabolism in heart disease: an epiphenomenon or a real culprit? Cardiovasc. Res. *90*, 220–223. https://doi.org/10.1093/cvr/cvr070.
23. McBrayer, S.K., Mayers, J.R., DiNatale, G.J., Shi, D.D., Khanal, J., Chakraborty, A.A., Sarosiek, K.A., Briggs, K.J., Robbins, A.K., Sewastianik, T., et al. (2018). Transaminase inhibition by 2-Hydroxyglutarate impairs glutamate biosynthesis and redox homeostasis in glioma. Cell *175*, 101–116.e25. https://doi.org/10.1016/j.cell.2018.08.038.
24. Raffel, S., Falcone, M., Kneisel, N., Hansson, J., Wang, W., Lutz, C., Bullinger, L., Poschet, G., Nonnenmacher, Y., Barnert, A., et al. (2017). BCAT1 restricts αKG levels in AML stem cells leading to IDHmut-like DNA hypermethylation. Nature *551*, 384–388. https://doi.org/10.1038/nature24294.
25. Li, J.T., Yin, M., Wang, D., Wang, J., Lei, M.Z., Zhang, Y., Liu, Y., Zhang, L., Zou, S.W., Hu, L.P., et al. (2020). BCAT2-mediated BCAA catabolism is critical for development of pancreatic ductal adenocarcinoma. Nat. Cell Biol. *22*, 167–174. https://doi.org/10.1038/s41556-019-0455-6.
26. Ericksen, R.E., Lim, S.L., McDonnell, E., Shuen, W.H., Vadiveloo, M., White, P.J., Ding, Z., Kwok, R., Lee, P., Radda, G.K., et al. (2019). Loss of BCAA catabolism during carcinogenesis enhances mTORC1 activity and promotes tumor development and progression. Cell Metab. *29*, 1151–1165.e6. https://doi.org/10.1016/j.cmet.2018.12.020.
27. Ananieva, E.A., Powell, J.D., and Hutson, S.M. (2016). Leucine metabolism in T cell activation: mTOR signaling and beyond. Adv. Nutr. *7*, 798s–805s. https://doi.org/10.3945/an.115.011221.
28. Yang, C., Khanniche, A., DiSpirito, J.R., Ji, P., Wang, S., Wang, Y., and Shen, H. (2016). Transcriptome signatures reveal rapid induction of

immune-responsive genes in human memory CD8(+) T cells. Sci. Rep. *6*, 27005. https://doi.org/10.1038/srep27005.

29. Wen, S., Lu, H., Wang, D., Guo, J., Dai, W., and Wang, Z. (2021). TCF-1 maintains CD8(+) T cell stemness in tumor microenvironment. J. Leukoc. Biol. *110*, 585–590. https://doi.org/10.1002/jlb.5mr1120-778r.
30. Ye, Z., Wang, S., Zhang, C., and Zhao, Y. (2020). Coordinated modulation of energy metabolism and inflammation by branched-chain amino acids and fatty acids. Front. Endocrinol. *11*, 617. https://doi.org/10.3389/fendo.2020.00617.
31. Link, W. (2019). Introduction to FOXO Biology. Methods Mol. Biol. *1890*, 1–9. https://doi.org/10.1007/978-1-4939-8900-3_1.
32. Wang, D., Wang, Y., Zou, X., Shi, Y., Liu, Q., Huyan, T., Su, J., Wang, Q., Zhang, F., Li, X., and Tie, L. (2020). FOXO1 inhibition prevents renal ischemia-reperfusion injury via cAMP-response element binding protein/PPAR-$\gamma$ coactivator-1$\alpha$-mediated mitochondrial biogenesis. Br. J. Pharmacol. *177*, 432–448. https://doi.org/10.1111/bph.14878.
33. Siebeneicher, H., Cleve, A., Rehwinkel, H., Neuhaus, R., Heisler, I., Müller, T., Bauser, M., and Buchmann, B. (2016). Identification and optimization of the first highly selective GLUT1 inhibitor BAY-876. ChemMedChem *11*, 2261–2271. https://doi.org/10.1002/cmdc.201600276.
34. Ojelabi, O.A., Lloyd, K.P., Simon, A.H., De Zutter, J.K., and Carruthers, A. (2016). WZB117 (2-Fluoro-6-(m-hydroxybenzoyloxy) Phenyl m-Hydroxybenzoate) inhibits GLUT1-mediated sugar transport by binding reversibly at the exofacial sugar binding site. J. Biol. Chem. *291*, 26762–26772. https://doi.org/10.1074/jbc.M116.759175.
35. Jung, M.K., Okekunle, A.P., Lee, J.E., Sung, M.K., and Lim, Y.J. (2021). Role of branched-chain amino acid metabolism in tumor development and progression. J. Cancer Prev. *26*, 237–243. https://doi.org/10.15430/jcp.2021.26.4.237.
36. Petro, T.M., and Bhattacharjee, J.K. (1981). Effect of dietary essential amino acid limitations upon the susceptibility to Salmonella typhimurium and the effect upon humoral and cellular immune responses in mice. Infect. Immun. *32*, 251–259. https://doi.org/10.1128/iai.32.1.251-259.1981.
37. Zhenyukh, O., Civantos, E., Ruiz-Ortega, M., Sánchez, M.S., Vázquez, C., Peiró, C., Egido, J., and Mas, S. (2017). High concentration of branched-chain amino acids promotes oxidative stress, inflammation and migration of human peripheral blood mononuclear cells via mTORC1 activation. Free Radic. Biol. Med. *104*, 165–177. https://doi.org/10.1016/j.freeradbiomed.2017.01.009.
38. Matsumura, T., Morinaga, Y., Fujitani, S., Takehana, K., Nishitani, S., and Sonaka, I. (2005). Oral administration of branched-chain amino acids activates the mTOR signal in cirrhotic rat liver. Hepatol. Res. *33*, 27–32. https://doi.org/10.1016/j.hepres.2005.07.001.
39. Nishida, M., Yamashita, N., Ogawa, T., Koseki, K., Warabi, E., Ohue, T., Komatsu, M., Matsushita, H., Kakimi, K., Kawakami, E., et al. (2021). Mitochondrial reactive oxygen species trigger metformin-dependent antitumor immunity via activation of Nrf2/mTORC1/p62 axis in tumor-infiltrating CD8T lymphocytes. J. Immunother. Cancer *9*, e002954. https://doi.org/10.1136/jitc-2021-002954.
40. Cham, C.M., and Gajewski, T.F. (2005). Glucose availability regulates IFN-gamma production and p70S6 kinase activation in CD8+ effector T cells. J. Immunol. *174*, 4670–4677. https://doi.org/10.4049/jimmunol.174.8.4670.
41. Elia, I., and Haigis, M.C. (2021). Metabolites and the tumour microenvironment: from cellular mechanisms to systemic metabolism. Nat. Metab. *3*, 21–32. https://doi.org/10.1038/s42255-020-00317-z.
42. Pavlova, N.N., and Thompson, C.B. (2016). The emerging hallmarks of cancer metabolism. Cell Metab. *23*, 27–47. https://doi.org/10.1016/j.cmet.2015.12.006.
43. Sugiura, A., and Rathmell, J.C. (2018). Metabolic barriers to T cell function in tumors. J. Immunol. *200*, 400–407. https://doi.org/10.4049/jimmunol.1701041.
44. Juric, V., O'Sullivan, C., Stefanutti, E., Kovalenko, M., Greenstein, A., Barry-Hamilton, V., Mikaelian, I., Degenhardt, J., Yue, P., Smith, V., and Mikels-Vigdal, A. (2018). MMP-9 inhibition promotes anti-tumor immunity through disruption of biochemical and physical barriers to T-cell trafficking to tumors. PLoS One *13*, e0207255. https://doi.org/10.1371/journal.pone.0207255.
45. Wang, T., Gnanaprakasam, J.N.R., Chen, X., Kang, S., Xu, X., Sun, H., Liu, L., Rodgers, H., Miller, E., Cassel, T.A., et al. (2020). Inosine is an alternative carbon source for CD8(+)-T-cell function under glucose restriction. Nat. Metab. *2*, 635–647. https://doi.org/10.1038/s42255-020-0219-4.
46. Li, Y., Gruber, J.J., Litzenburger, U.M., Zhou, Y., Miao, Y.R., LaGory, E.L., Li, A.M., Hu, Z., Yip, M., Hart, L.S., et al. (2020). Acetate supplementation restores chromatin accessibility and promotes tumor cell differentiation under hypoxia. Cell Death Dis. *11*, 102. https://doi.org/10.1038/s41419-020-2303-9.
47. Vega, O.M., Abkenari, S., Tong, Z., Tedman, A., and Huerta-Yepez, S. (2021). Omega-3 polyunsaturated fatty acids and lung cancer: nutrition or pharmacology? Nutr. Cancer *73*, 541–561. https://doi.org/10.1080/01635581.2020.1761408.
48. Peng, H., Wang, Y., and Luo, W. (2020). Multifaceted role of branched-chain amino acid metabolism in cancer. Oncogene *39*, 6747–6756. https://doi.org/10.1038/s41388-020-01480-z.

## STAR★METHODS

### KEY RESOURCES TABLE

| REAGENT or RESOURCE | SOURCE | IDENTIFIER |
|---|---|---|
| Antibodies | | |
| Fixable viability stain 510 | BD Biosciences | Cat# 564406; RRID: AB_2869572 |
| APC-Cy™7 Rat Anti-Mouse CD45 (30-F11) | BD Biosciences | Cat# 557659; RRID: AB_396774 |
| BV711 Hamster Anti-Mouse CD3e (145-2C11) | BD Biosciences | Cat# 563123; RRID: AB_2687954 |
| BV650 Rat Anti-mouse CD8a (53-6.7) | Biolegend | Cat# 100742; RRID: AB_2563056 |
| PerCP-Cy™5.5 Rat Anti-Mouse CD45R/B220 (RA3-6B2) | BD Biosciences | Cat# 552771; RRID: AB_394457 |
| FITC Mouse Anti-Mouse NK1.1(PK136) | eBioscience | Cat# 11-5941-82; RRID: AB_465318 |
| FITC Rat Anti-Mouse CD44 (IM7) | BD Biosciences | Cat# Cat# 553133; RRID: AB_2076224 |
| APC-R700 Rat Anti-Mouse CD62L (MEL-14) | BD Biosciences | Cat# 565159; RRID: AB_2737397 |
| FITC Rat Anti-Mouse IFN-γ (XMG1.2) | BD Biosciences | Cat# 554411; RRID: AB_395375 |
| PE-Cyanine7 Rat Anti-Mouse TNF alpha (MP6-XT22) (MP6-XT22) | eBioscience | Cat# 25-7321-82; RRID: AB_11042728 |
| FITC Rat Anti-Mouse CD107a (1D4B) | BD Biosciences | Cat# 553793; RRID: AB_395057 |
| PE Rat Anti-Mouse Granzyme B (NGZB) | Invitrogen | Cat# 12-8898-82; RRID: AB_10870787 |
| BV786 Mouse Anti-Mouse CD366 (TIM-3) (7D3) | BD Biosciences | Cat# 747621; RRID: AB_2744187 |
| PE Rat Anti-Mouse TOX (TXRX10) | Invitrogen | Cat# 12-6502-82; RRID: AB_10855034 |
| BV421 Mouse Anti-TCF-7/TCF-1 (S33-966) | BD Biosciences | Cat# 566692; RRID: AB_2869822 |
| PE/Cyanine7 Rat Anti-mouse CD185 (CXCR5) (L138D7) | Biolegend | Cat# 145516; RRID: AB_2562210 |
| Alexa Fluor® 647 Rabbit Anti-Mouse GLUT1 (EPR3915) | Abcam | Cat# ab195020; RRID: AB_2783877 |
| APC Hamster Anti-Mouse CD279 (PD-1) (J43) | BD Biosciences | Cat# 562671; RRID: AB_2737712 |
| BV421 Hamster Anti-Mouse CD279 (PD-1) (J43) | BD Biosciences | Cat# 562584; RRID: AB_2737668 |
| BV510 Mouse Anti-Human CD3 (HIT3a) | BD Biosciences | Cat# 564713; RRID: AB_2738909 |
| APC Mouse Anti-human CD8a (RPA-T8) | Biolegend | Cat# 301014; RRID: AB_314132 |
| APC/Cyanine7 Mouse Anti-human TNF-α (MAb11) | Biolegend | Cat# 502944; RRID: AB_2562870 |
| FITC Mouse anti-Human Granzyme B (GB11) | BD Biosciences | Cat# 560211; RRID: AB_1645488 |
| PE Mouse Anti-Human Glut1 (202,915) | BD Biosciences | Cat# FAB1418P; RRID: AB_2191040 |
| FITC Mouse Anti-Human CD45RO (UCHL1) | BD Biosciences | Cat# 555492; RRID: AB_395883 |
| APC-H7 Mouse Anti-Human CD27 (M-T271) | BD Biosciences | Cat# 560222; RRID: AB_1645474 |
| *InVivo*Mab anti-mouse PD-1(CD279) (RMP1-14) | BioXCell | Cat# BE0146; RRID: AB_10949053 |
| *InVivo*Mab anti-mouse CD8α (YTS 169.4) | BioXCell | Cat# BE0117; RRID: AB_10950145 |
| Rabbit Anti-Mouse Phospho-p70 S6 Kinase (Thr389) (108D2) | CST | Cat# 9234; RRID: AB_2269803 |
| Rabbit Anti-Mouse β-Actin (13E5) | CST | Cat# 4970; RRID: AB_2223172 |
| Rabbit Anti-Mouse Phospho-Akt (Ser473) (D9E) | CST | Cat# 4060; RRID: AB_2315049 |
| Rabbit Anti-Mouse PI3 Kinase p85 (19H8) | CST | Cat# 4257; RRID: AB_659889 |
| Rabbit Anti-Mouse Phospho-FoxO1 (Ser256) | CST | Cat# 9461; RRID: AB_329831 |
| Mouse PD-L1/B7-H1 Antibody | RD | Cat# AF1019; RRID: AB_354540 |
| Anti-CD8 alpha Rabbit pAb antibody | Servicebio | Cat# GB11068; RRID: AB_2905511 |
| Anti-GLUT1 Rabbit pAb antibody | Servicebio | Cat# GB11066 |
| Cy3 conjugated Donkey Anti-Goat IgG (H + L) antibody | Servicebio | Cat# GB21404; RRID: AB_2868507 |
| Cy3 conjugated Goat Anti-Rabbit IgG antibody | Servicebio | Cat# GB21303; RRID: AB_2861435 |

(*Continued on next page*)

*Continued*

| REAGENT or RESOURCE | SOURCE | IDENTIFIER |
|---|---|---|
| FITC-labeled goat anti-rabbit IgG antibody | Servicebio | Cat# GB22303; RRID: AB_2904189 |
| **Chemicals, peptides, and recombinant proteins** | | |
| Phorbol 12-myristate 13-acetate | Sigma-Aldrich | Cat# P1585 |
| Ionomycin calcium salt | Sigma-Aldrich | Cat# I3909 |
| Fixation/Permeabilization Solution | | N/A |
| Kit with BD GolgiStop™ | BD Biosciences | Cat# 554715 |
| Transcription Factor Buffer Set | BD Biosciences | Cat# 562574 |
| Leucine | Sigma-Aldrich | Cat# L8000 |
| Valine | Sigma-Aldrich | Cat# V5013 |
| Isoleucine | Sigma-Aldrich | Cat# I2752 |
| 2-Deoxy-D-glucose | Sigma-Aldrich | Cat# D6134 |
| Oligomycin | Sigma-Aldrich | Cat# O4876 |
| AS1842856 | Selleck | Cat# S8222 |
| Sanguinarine chloride | Selleck | Cat# S5452 |
| WZB117 | Selleck | Cat# S7927 |
| Rapamycine | Selleck | Cat# S1039 |
| Lymphoprep | Serumwerk Bernburg AG | Cat# 1858 |
| Mouse Recombinant IL-2 | Stemcell | Cat# 78081 |
| Foundation Fetal Bovine Serum | Gemini | Cat# 900-108 |
| Dulbecco's Modified Eagle Medium (DMEM) | HyClone | Cat# SH30243.01 |
| RPMI 1640 medium | HyClone | Cat# SH30809.01 |
| Phosphate Buffered Saline | HyClone | Cat# SH30256.01 |
| Dulbecco's Modified Eagle Medium (DMEM) without D-Glucose | Thermo Fisher Scientific | Cat# 11966025 |
| RPMI 1640 medium without L-leucine, L-valine, L-isoleucine | BasalMedia | Cat# X054E1 |
| Penicillin/Streptomycin | Thermo Fisher Scientific | Cat# 15140122 |
| L-Glutamine | Thermo Fisher Scientific | Cat# 25030081 |
| HEPES Buffer Solution | Thermo Fisher Scientific | Cat# 15630080 |
| MEM Non-Essential Amino Acids Solution | Thermo Fisher Scientific | Cat# 11140050 |
| 2-mercaptoethanol | Thermo Fisher Scientific | Cat# 21985023 |
| Universal tissue fixative | Servicebio | Cat# G1101 |
| Sucrose | Sinopharm Group Chemical Reagent Co. LTD | Cat# 57-50-1 |
| OCT embedding agent | Servicebio | Cat# G6059 |
| DAPI | Servicebio | Cat# 1012 |
| RIPA Buffer | Thermo Fisher Scientific | Cat# 89901 |
| PMSF | Thermo Fisher Scientific | Cat# 36978 |
| TRIzol | Thermo Fisher Scientific | Cat# 15596018 |
| PrimeScript™ RT reagent Kit | Takara | Cat# RR037B |
| TB Green™ Premix Ex Taq™ II | Takara | Cat# RR82WR |
| **Critical commercial assays** | | |
| Cytotoxicity LDH Assay Kit-WST | Dojindo | Cat# CK12 |
| XF Glycolytic stress test kit | Agilent Technologies | Cat# 103020-100 |
| XF Cell Mito stress test kit | Agilent Technologies | Cat# 103015-100 |
| EasySep™ Human CD8+T cell Isolation Kit | Stemcell | Cat# 19853A |
| EasySep™ Human CD8 Positive Selection Kit II | Stemcell | Cat# 17853 |
| Glucose Assay Kit | Abcam | Cat# ab65333 |

(*Continued on next page*)

*Continued*

| REAGENT or RESOURCE | SOURCE | IDENTIFIER |
|---|---|---|
| L-Lactate Assay Kit (Colorimetric/Fluorometric) | Abcam | Cat# ab65330 |
| Dynabeads™Mouse T-Activator CD3/CD28 | Thermo Fisher Scientific | Cat# 11452D |
| Dynabeads™ Human T-Activator CD3/CD28 | Thermo Fisher Scientific | Cat# 11131D |
| Tumor Dissociation Kit | MiltenyiBiotec | Cat# 130-096-730 |
| GentleMACS 25 C Tubes | MiltenyiBiotec | Cat# 130-093-237 |
| MACS SmartStrainer | MiltenyiBiotec | Cat# 130-098-462 |
| AllPrep DNA/RNA/miRNA Universal Kit | QIAGEN | Cat# 80224 |
| Dynabeads mRNA DIRECT Micro kit | Invitrogen | Cat# 61021 |
| KAPA Stranded RNA-Seq Library Preparation Kit | KAPA | Cat# KK8400 |
| Protein Assay Kit I | Bio-Rad | Cat# 5000001 |
| **Deposited data** | | |
| RNA-sequencing data | deposited in Gene Expression Omnibus | GEO: GSE224250 |
| **Experimental models: Cell lines** | | |
| Mouse B16-F10 melanoma cells | ATCC | CRL-6475, RRID: CVCL_0159 |
| Mouse Lewis lung carcinoma line | ATCC | CRL-1642, RRID: CVCL_4358 |
| **Oligonucleotides** | | |
| ACTIN-F | AGAAGGACTCCTATGTGGGTGA | N/A |
| ACTIN-R | CATGAGCTGGGTCATCTTTTCA | N/A |
| CPT1A-F | CTCCGCCTGAGCCATGAAG | N/A |
| CPT1A-R | CACCAGTGATGATGCCATTCT | N/A |
| ACAA2-F | CTGCTACGAGGTGTGTTCATC | N/A |
| ACAA2-R | AGCTCTGCATGACATTGCCC | N/A |
| ECHS1-F | TTGTGAACTTGCCATGATGTGT | N/A |
| ECHS1-R | TGCTCGGGTGAGTCTCTGAG | N/A |
| ACSS1-F | GTTTGGGACACTCCTTACCATAC | N/A |
| ACSS1-R | AGGCAGTTGACAGACACATTC | N/A |
| ACSS2-F | AAACACGCTCAGGGAAAATCA | N/A |
| ACSS2-R | ACCGTAGATGTATCCCCCAGG | N/A |
| **Software and algorithms** | | |
| FlowJo v.10.CL | FlowJo | https://www.flowjo.com/ |
| Prism v.8.0 | GraphPad | http://www.graphpad.com |
| ImageJ | NIH | https://imagej.nih.gov/ij/ |
| MetaboAnalyst 4.0 | N/A | https://www.metaboanalyst.ca/ |
| **Other** | | |
| Seahorse XFe96 Extracellular Flux Analyzer | Agilent Technologies | N/A |
| BD LSRFortessa X20 | BD Biosciences | N/A |
| Amersham Imager 600 | GE | N/A |
| Leica Sp8 laser scanning confocal microscope | Leica Biosystems | N/A |
| Frozen section machine | Thermo Fisher Scientific | N/A |

## RESOURCE AVAILABILITY

### Lead contact

Further information and requests for resources and reagents should be directed to and will be fulfilled by the lead contact, Ying Wang (ywangssmu@shsmu.edu.cn).

### Materials availability

All materials generated in this study are available from the lead contact.

### Data and code availability

- The RNA sequencing dataset generated during this study has been submitted in the Gene Expression Omnibus under the accession number GSE224250.
- This paper does not report original code.
- Any additional information required to reanalyze the data reported in this paper is available from the lead contact upon request.

## EXPERIMENTAL MODEL AND SUBJECT DETAILS

### Human subjects

Patients enrolled in this study were those with advanced NSCLC participating in two clinical trials (CheckMate 078 [NCT02613507] and CheckMate870 [NCT03195491]) in Shanghai Chest Hospital affiliated to Shanghai Jiao Tong University School of Medicine. Patients enrolled were at stage IIIB/IV with disease progression after one to two prior systemic therapies. All participants had measurable disease severity by computed tomography (CT) or magnetic resonance imaging (MRI) using Response Evaluation Criteria in Solid Tumors version 1.1 (RECIST 1.1). Patients received nivolumab 3 mg/kg intravenously every 2 weeks until disease progression or intolerable toxicity. Responses to the treatment were evaluated every 6 weeks and were confirmed by a subsequent assessment no less than 4 weeks from the date firstly documented. Patients in this study were defined as the responder (R) (with PFS >180 days) or the non-responder (NR) (with PFS <180 days) according to the RECIST 1.1 evaluation. The study was approved by the Ethics Committee of Shanghai Chest Hospital. All patients were informed of the study, consented to the enrollment, and signed an informed consent form. All the procedures were conducted following the Declaration of Helsinki. The basic information of NSCLC patients included in this study summarized in Table S1. Healthy donors were healthy volunteers.

### Mice

*PP2Cm* germ-line knockout (KO) mice with C57BL/6 background were generated as previously described[13] and maintained in a specific pathogen-free (SPF) animal facility of Shanghai Jiaotong University School of Medicine (SJTUSM). Wild-type (WT) mice used in some experiments were purchased from the Shanghai Laboratory Animal Center (Shanghai, China) and maintained under specific-pathogen-free (SPF) conditions in the animal facility of SJTUSM. Mice were subjected to 12 h light/dark cycles (light cycle from 6 am to 6 pm and dark cycle from 6 pm to 6 am) and were maintained at stable room temperature between 68 and 72°F, with food and water. For all experiments, 6-8-week-old sex-matched mice were used unless otherwise indicated. All animal experiments were approved by the Institutional Animal Care and Use Committee (IACUC) of Shanghai Jiao Tong University School of Medicine (A-2022-018). Age and sex-matched *Rag1*$^{-/-}$ mice were purchased from The GemPharmatech LLC (Nanjing, China)

### Cells lines

The Lewis lung carcinoma cell line (LLC) and B16-F10 melanoma cell line were purchased from the American Type Culture Collection (ATCC) previously and maintained in complete Dulbecco's Modified Eagle Medium (DMEM, ThermoFisher Scientific Inc.) containing 10% fetal bovine serum (FBS, Gemini Inc.) and 1% penicillin/streptomycin (P/S, ThermoFisher Scientific Inc.) at 37°C with 5% $CO_2$ atmosphere. B16-F10 and LLC cells were used in mouse tumor models, and *in vitro* proliferation and cytotoxicity assay.

## METHOD DETAILS

### Mouse tumor models

For tumor models, tumor cells were injected subcutaneously (s.c.) into 8-week-old mice ($2 \times 10^5$ B16-F10 cells or $5 \times 10^5$ LLC cells per mouse). Tumor volumes were monitored from Day 7 and were calculated by using the equation (length x width$^2$)/2. Calculation of tumor volumes was done in a blinded fashion and the lethality was defined as tumor volumes reaching 1500 mm$^2$.

For *Rag1*$^{-/-}$ adoptive transfer model, $1 \times 10^6$ purified CD8$^+$ T cells from the spleens of the mice fed with Normal BCAA or High BCAA water were injected (i.v.) 2 days before LLC tumor inoculation.

### *In vivo* anti-PD-1 treatment

For *in vivo* anti-PD-1 treatment, 200 μg/100 μL purified anti-PD-1 monoclonal antibodies (RMP1-14, BioXcell) were intraperitoneal (i.p.) injected on day 10, 13 and 16 in LLC-implanted mice ($5 \times 10^5$ LLC cells were injected on Day 0), and on day 7, 10 and 13 in B16-F10-implanted mice ($2 \times 10^5$ B16-F10 cells were injected on Day 0). Control mice were treated with i.p. injection of 100 μL PBS.

### *In vivo* high or low BCAA-fed mouse model

In high BCAA-fed experiments, mice were fed with water containing 15 mg/mL valine, 15 mg/mL leucine and 15 mg/mL isoleucine throughout the whole experiment while control mice (normal BCAA) were fed with normal sterile dd$H_2O$. Blood was collected via the Posterior ophthalmic venous plexus for BCAA level measurement. In low BCAA-fed experiments, low BCAA-diet was purchased from XIETONGSHENGWU (Nanjing, China).

### *In vivo* T cell depletion

For *In vivo* depletion of $CD8^+$ T cells, 200 μg/100 μL purified anti-CD8 monoclonal antibodies (YTS 169.4, BioXCell) were intraperitoneal (i.p.) injected on day −2, 5 and 12 respectively and $5 \times 10^5$ LLC cells or $2 \times 10^5$ B16-F10 cells were injected on Day 0. Control mice were treated with *i.p*. injection of 100 μL PBS.

### Preparation of mouse tumor infiltrating lymphocytes

Grafted tumors were minced into small pieces and put into Macs C tubes (MiltenyiBiotec) followed by enzymatic digestion in FBS-free DMEM culture medium containing 16 mg/mL Enzyme D, 0.4 mg/mL Enzyme R and 0.5 mg/mL Enzyme A (all from MiltenyiBiotec). Cell suspensions were successively filtered through 70 mm cell strainers (MiltenyiBiotec) to obtain single cell suspension and subjected to further experiments.

### Isolation of mouse $CD8^+$ T cells and *in vitro* stimulation

Mouse spleens and lymph nodes were homogenized and lymphocytes were prepared by density gradient centrifugation using Lymphoprep (Serumwerk Bernburg AG). $CD8^+$ T cells were purified by MACS beads (Stem cell) according to the manufacturer's instructions. The purity was >95% confirmed by flow cytometric analysis. Purified $CD8^+$ T cells were stimulated with anti-CD3/CD28 beads (Thermo Fisher Scientific) for 24 h in complete RPMI 1640 medium (Hyclone) supplemented with 10% fetal bovine serum (Gemini), 1% penicillin/streptomycin (P/S, Thermo Fisher Scientific), 1% L-glutamine (Thermo Fisher Scientific), 1% HEPES Buffer Solution (Thermo Fisher Scientific), 1% MEM Non-Essential Amino Acids Solution (Thermo Fisher Scientific) and 0.1% 2-mercaptoethanol (Thermo Fisher Scientific) at 37°C with 5% $CO_2$. For glucose uptake and lactate production detection, IL-2 (10 ng/mL, Stem Cell) was added additionally during $CD8^+$ T cell stimulation. For *in vitro* inhibition experiments, 5 mM 2-DG (Sigma-Aldrich), 10 μM Oligomycin (Sigma-Aldrich), 10 μM WZB117 (Selleck), 1 μM AS1842856 (Selleck), 1 μM Sanguinarine chloride (Selleck) and 100 nM Rapamycin (Selleck) were added during $CD8^+$ T cell stimulation. For *in vitro* BCAA supplementation experiment, valine, leucine and isoleucine (all from Sigma-Aldrich) were added in BCAA-free RPMI medium (Basal Media) at the concentration of 10 mM for $CD8^+$ T cell stimulation.

### Preparation of human $CD8^+$ T cells and *in vitro* stimulation

Human peripheral blood mononuclear cells (PBMCs) were prepared by gradient centrifugation using Lymphoprep (Serumwerk Bernburg AG) and washed with RPMI 1640 culture medium. $CD8^+$ T cells were purified by MACS beads (StemCell) according to the manufacturer's instructions. The purity was >90% confirmed by flow cytometry. Purified $CD8^+$ T cells were stimulated with anti-CD3/CD28 beads (Thermo Fisher Scientific) for 24 h with BCAAs at gradient concentrations.

### Flow cytometry

For the analysis on surface markers, mouse TILs or splenocytes were stained in PBS containing 2% FBS (FACS buffer) with FVS (BV510) and antibodies targeting mouse CD45 (Apc-cy7), CD3e (BV711), CD8a (BV650), B220 (Percp-cy5.5), NK1.1 (FITC), CD44 (BV785), CD62L (APC-R700), PD-1 (BV421), Tim-3 (BV786) and CXCR5 (PE-cy7), incubated for 35 min at 4°C, washed once with FACS buffer and fixed in PBS containing 1% paraformaldehyde. For human PBMC staining, antibodies targeting CD3 (Bv510), CD8a (APC), CD45RO (FITC) and CD27 (Apc-h7) were used.

For intracellular cytokine detection, cells were stimulated with phorbol 12-myristate 13-acetate (PMA, 100 ng/mL, Sigma-Aldrich), ionomycin (1 mg/mL, Sigma-Aldrich) and GolgiStop™ (0.1%, BD Biosciences) for 4 h. After the stimulation, cells were stained with antibodies targeting surface molecules and subject to intracellular staining by using Cytofix/Cytoperm™ Kit (BD Biosciences) according to the manufacturer's instructions. Briefly, cells were fixed and permeabilized, and followed by adding antibodies targeting IFN-γ (APC-cy7), TNF-α (PE-cy7), CD107A (FITC), GzmB (PE), Glut1 (Alexa 647) for mouse lymphocytes and TNF-α (APC-cy7), Gzm B (FITC), Glut1 (PE) for human lymphocytes.

For intracellular transcriptional factor staining, cells were firstly labeled with surface markers before fixation/permeabilization with BD Pharmingen™ Transcription Factor Kit (BD Biosciences) and then stained with antibodies targeting TCF-7 (BV421), TOX (PE), PD-1 (APC) and Tim-3 (BV786).

Cells were acquired on a BD LSR Fortessa X20 (Beckton Dicknson). Data were analyzed with FlowJo Version 10.0 software.

### Cell proliferation assay

Cell Counting Kit-8 detection kit (Dojindo) was used to determine the proliferation of tumor cells. In brief, LLC and B16-F10 cells were diluted to the concentration of 30,000 cells/mL. 100 μL cell suspension was added to replicate in 96-well plates and cultured for 0, 24, 48, and 72 h respectively. 10 μL CCK-8 reagent was added to each well followed by incubation for 4 h at 37°C. The absorbance at 450 nm was measured using a PowerWaveXS2 microplate spectrophotometer (BioTek Instruments, Inc., VT, USA).

### RNA-sequencing analysis

Purified wild-type (WT) and *PP2Cm*$^{-/-}$ $CD8^+$ T cells were stimulated with anti-CD3/CD28 beads for 24 h. Total RNA was extracted using AllPrep DNA/RNA/miRNA Universal Kit (QIAGEN). mRNA was further purified by using Dynabeads mRNA DIRECT Micro kit (Invitrogen) and subjected to library preparation using KAPA Stranded RNA-Seq Library Preparation Kit (KAPA). The libraries were

multiplexed and sequenced on Illumina Nextseq500 (75bp paired-end reads). Raw FASTQ files from RNA-seq assay were aligned to the GRCm38 reference genome using Kallisto (https://pachterlab.github.io/kallisto/), filtered to remove transcripts with low counts, and trimmed using the FPKM normalization method. Only transcripts with mean count number >10 were analyzed. To define transcriptional differences between *PP2Cm*$^{-/-}$ and WT CD8$^{+}$ T cells, the intersection of genes of significant differentiation expression (DEGs) from Limma, DESeq2, and EdgeR R packages (R version: 3.8.0) was extracted for volcano plot, and a false discovery rate (FDR) q-value of 0.01 and Log2 fold change of 1 were imposed as the cut-off.

### Enrichment analysis

Pathway enrichment was calculated using several biological databases (KEGG, Reactome, Biocarta, and Panther) with an FDR q-value <0.01. Metabolism-related pathways were further enriched according to 61 metabolic genes from the KEGG database as have been indicated in previous reports. For gene set enrichment analysis (GSEA) analysis, GSE9650_EXHAUSTED_VS_MEMORY_CD8_T cell_DN, GOBP_T_CELL_ACTIVATION, KEGG_OXIDATIVE_PHOSPHORYLATION, HALLMARK_GLYCOLYSIS

REACTOME and GOBP_FATTY_ACID_BETA_OXIDATION were performed using GSEA based R package.

### Western blot assay

Cells were washed with ice-cold PBS and lysed on ice for 30 min in RIPA buffer (Thermo Fisher Scientific) containing 1mM Phenylmethanesulfonylfluoride (PMSF) (Thermo Fisher Scientific). Whole-cell extracts were collected by centrifugation and protein concentration was determined by BCA protein assay kit (Bio-Rad Laboratories, CA, USA). Cell lysates were subjected to 10% sodium dodecyl sulfate-polyacrylamide gel electrophoresis (SDS-PAGE) and transferred to polyvinylidene difluoride (PVDF) membranes (Millipore, MA, USA) by semi-dry transfer system. The membranes were blocked with PBS (pH7.4) containing 5% non-fat dried milk for 2 h at room temperature and then incubated with primary antibodies overnight at 4°C. After incubation with HRP-conjugated secondary antibodies for 1 h, immunoreactive proteins were visualized with ECL detection system (Millipore).

### Immunofluorescence analysis

Fresh tumor tissues were fixed in Universal tissue fixative (Servicebio, Wuhan, China) for more than 24 h. The tissues were removed to 15% sucrose solution (Sinopharm Group Chemical Reagent Co. LTD) at 4°C for 12 h, and 30% sucrose solution at 4°C for 12 h for dehydration. Dehydrated tissues were embedded in the OCT embedding agent (Servicebio) and frozen at −20°C. 8–10 μM sections were sliced on clean slides and subjected to immunofluorescence assay. Briefly, PBS-3% BSA was added to the tissues to block non-specific binding for 30 min and anti-mouse PD-L1 pAb (1:150), anti-mouse CD8α pAb (1:300) or anti-mouse Glut1 pAb (1:300) were incubated with the tissues at 4°C overnight in a wet box. The slides were rinsed three times with PBS (pH 7.4) and incubated with AF488-goat anti-rabbit (1:400), Cy3-donkey anti-Goat (1:300), or Cy3-goat anti-rabbit pAbs (1:300) at room temperature for 50 min in dark. The slides were washed three times with PBS (pH 7.4) for 5 min each. DAPI solution (1:5000) was added for counterstain and mounted using Vectashield fluorescence media. Slides were imaged using Leica Sp8 laser scanning confocal microscope and analyzed by using the ImageJ website online (https://imagej.nih.gov/ij/).

### Lactate dehydrogenase (LDH) release assay

Cytotoxicity was performed by LDH release assay using CytoTox 96 Non-Radioactive Cytotoxicity assay kit (Dojindo) according to the manufacturer's instructions. Briefly, CD8$^{+}$ T cells were washed with sterile PBS (Hyclone), resuspended in serum-free RPMI 1640 as effector cells at 1 × 10$^{7}$/mL, and then mixed with LLC cells (1×10$^{5}$/mL) at different effector to target (E: T) ratios. After culturing for 4 h at 37°C, LDH release was detected and cytotoxicity was calculated according to the following formula:

Cytotoxicity (%) = 100 × (Experimental release – Target cell spontaneous release)/(Target cell maximum release-target cell spontaneous release).

"Experimental release" referred to LDH release from experimental wells. "Target cell spontaneous release" referred to the spontaneous release of LDH from target cells alone. "Target cell maximum release" referred to the maximum release of LDH from target cells in a medium containing 1% Triton X-100 T cells.

### Extracellular flux analysis

Glycolysis Stress Test (GST) and mitochondrial stress test (MST) were purchased from Agilent technologies, and Extracellular acidification rate (ECAR) and oxygen consumption rate (OCR) were measured using the Seahorse XF analyzer (Agilent Technologies) according to the manufacturer's instructions. Briefly, 2x10$^{5}$ activated T cells were plated in Cell-Tak (Corning)-coated XF96 plates in RPMI 1640 medium (pH 7.4) containing 2 mM L-glutamine only for GST, or supplemented with 10 mM glucose, 2 mM L-glutamine, and 1 mM sodium pyruvate for GRA and MST (all from Agilent technologies) via centrifugation to ensure cell attachment. Cells were equilibrated for 1 h in a non-$CO_2$ incubator before starting the assay. For GST, ECAR was measured under basal conditions and in response to 10 mM glucose, 1 μM Oligo, and 50 mM 2-DG successively to calculate the basal glycolytic rate, glycolytic capacity (in response to Oligo), and glycolytic reserve (=glycolytic capacity−basal rate). For MST, OCR was measured under basal conditions and in response to sequential injections of 1 μM Oligo, 1 μM FCCP (Carbonyl cyanide 4-trifluoromethoxyphenyl hydrazone), and 0.5 μM R/A to calculate basal respiration rate (=baseline OCR−R/A OCR), maximal respiration rate (=FCCP OCR−R/A OCR), Spare respiration capacity (=maximal respiration−basal respiration) and ATP production (=Basal Respiration-Proton Leak).

### Detection of glucose consumption and lactate production

Freshly isolated $CD8^+$ T cells were seeded in 24-well plates (3 x $10^6$/well) in RPMI 1640 medium and stimulated with anti-CD3/28 beads with the presence of 10 ng/mL IL-2 for 24 h. The supernatants were collected to detect glucose consumption by using Glucose Assay Kit (Abcam). Glucose uptake was calculated as the concentrations of glucose in the medium without the cells minus those in the medium after culturing cells for 24 h. Lactate production was detected by measuring lactate in the supernatants using a lactate Colorimetric/Fluorometric assay kit according to the manufacturer's instructions (Abcam).

### Metabolomic analysis

$CD8^+$ T cells were activated with anti-CD3/28 beads for 24 h. Cells were washed once with PBS and the metabolites were extracted from freshly activated $CD8^+$ T cells using 80% precooled methanol. After 20 min incubation at −80°C, the samples were centrifuged at 15,000 *rpm* for 10 min at 4°C to remove protein components. The supernatants were collected for target LC-MS/MS detection as described previously. Briefly, cell extracts were analyzed by ultra-high-performance liquid chromatography (Acquity, Waters) coupled to a Q Exactive hybrid quadrupole–orbitrap mass spectrometer (Thermo Fisher). The injection volume was 10 μL. Metabolites were separated with a Luna NH2 column (100 mm × 2 mm, 3 μm particle size, Phenomenex). The key parameters were as follows: ionization voltage, +3.8 kV/–3.0 kV; sheath gas pressure, 35 arbitrary units; auxiliary gas, 10 arbitrary units; auxiliary gas heater temperature, 350°C; capillary temperature, 320°C. The mass spectrometer was run in full scan mode at an m/z 70–1,000 scan range and 70,000 resolutions. Data processing and ion annotation based on accurate mass in Xcalibur 4.0 (Thermo Fisher). A subset of identified compounds was verified by mass and retentiontime match to authenticated standards. For the stable-isotope tracing experiment, freshly isolated $CD8^+$ T cells were activated with anti-CD3/28 beads in the medium containing 11 mM [U-$^{13}$C]-glucose for 24 h. Cells were washed with PBS once and subjected to LC-MS detection. To determine intermediate metabolites in WZB117 inhibitor assays, $CD8^+$ T cells were activated with anti-CD3/28 beads with the presence of 10 μM WZB117 for 24 h. Cells were collected and subjected to target LC-MS/MS detection.

### Luminex assay

The concentrations of IFN-γ in the serum were determined using a Luminex assay conducted by LAIZEE BIOTECH CO., LTD including 10 cytokines. Standard curves were generated from the mean fluorescent intensity (MFI) of reference cytokine gradient concentrations by using Luminex200 IS V2.1 Software. The concentrations of IFN-γ in serum samples were calculated according to the standard curves.

### RT-PCR

Total RNA of activated $CD8^+$ T cells was extracted with TRIzol (Thermo Fisher, Carlsbad, CA, USA) according to the manufacturer's protocol. Reverse transcription reactions were conducted using PrimeScript RT reagent Kit (Takara Bio, Tokyo, Japan) according to the manufacturer's instructions. Subsequently, 50 ng of cDNA was used as a qPCR template to quantify genes using TB Green Premix Ex Taq II (Takara Bio, Tokyo, Japan). Target genes related to fatty acid oxidation (the primers were listed in the key resources table) were amplified over 40 cycles at 95°C for 15 s, 60°C for 15 s, and 72°C for 45 s. Gene expressions were normalized to β-actin according to the cycle threshold ($2^{-\Delta\Delta CT}$) method.

## QUANTIFICATION AND STATISTICAL ANALYSIS

Data were presented as mean ± standard error of the mean (SEM). Statistical analysis was performed using Prism 8.0 software. Two-tailed unpaired Student's t t-tests were performed. Survival curves for the PFS were estimated using the Kaplan-Meier method (log rank test). The Spearman correlation test was applied to perform the association analysis. $p < 0.05$ was considered statistically significant.

**Cell Reports, Volume *42***

## Supplemental information

# Accumulation of branched-chain amino acids reprograms glucose metabolism in CD8$^+$ T cells with enhanced effector function and anti-tumor response

**Cheng-cheng Yao, Rui-ming Sun, Yi Yang, Hai-yan Zhou, Zhou-wenli Meng, Rui Chi, Li-liang Xia, Ping Ji, Ying-ying Chen, Guo-qing Zhang, Hai-peng Sun, Shun Lu, Chen Yang, and Ying Wang**

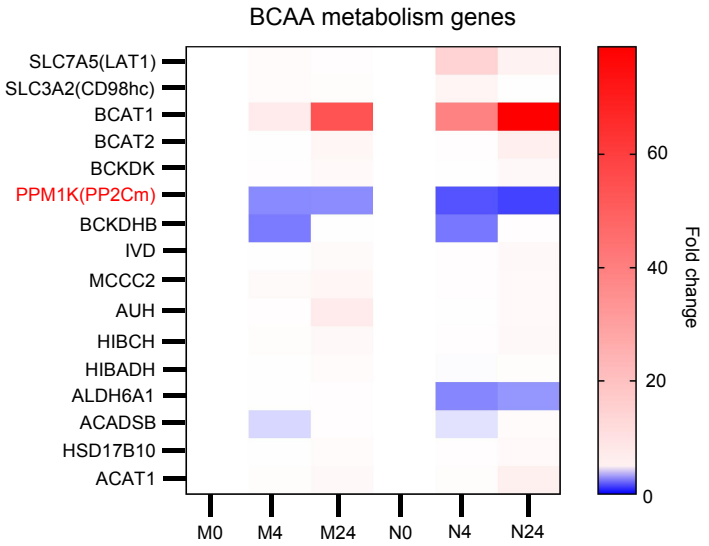


**Supplementary Figure 1. Downregulation of *PP2Cm* in human CD8⁺ T cells upon anti-CD3/CD28 activation.**

Memory and naive CD8⁺ T cells were purified from peripheral blood mononuclear cells of healthy donors, and were activated by anti-CD3/28 microbeads at the ratio of 1:1 *in vitro* for 4 h or 24 h. Activated cells were subject to transcriptome analysis by RNA sequencing. Genes related to BCAA metabolism were enriched in which *PP2Cm* was downregulated both in memory and naive CD8⁺ T cells after the activation.

M0: Memory CD8⁺ T cells without activation; M4: Memory CD8⁺ T cells upon anti-CD3/CD28 activation for 4 h; M24: Memory CD8⁺ T cells upon anti-CD3/CD28 activation for 24 h; N0: naive CD8⁺ T cells without activation; N4: Naive CD8⁺ T cells upon anti-CD3/CD28 activation for 4 h; N24: Memory CD8⁺ T cells upon anti-CD3/CD28 activation for 24 h.

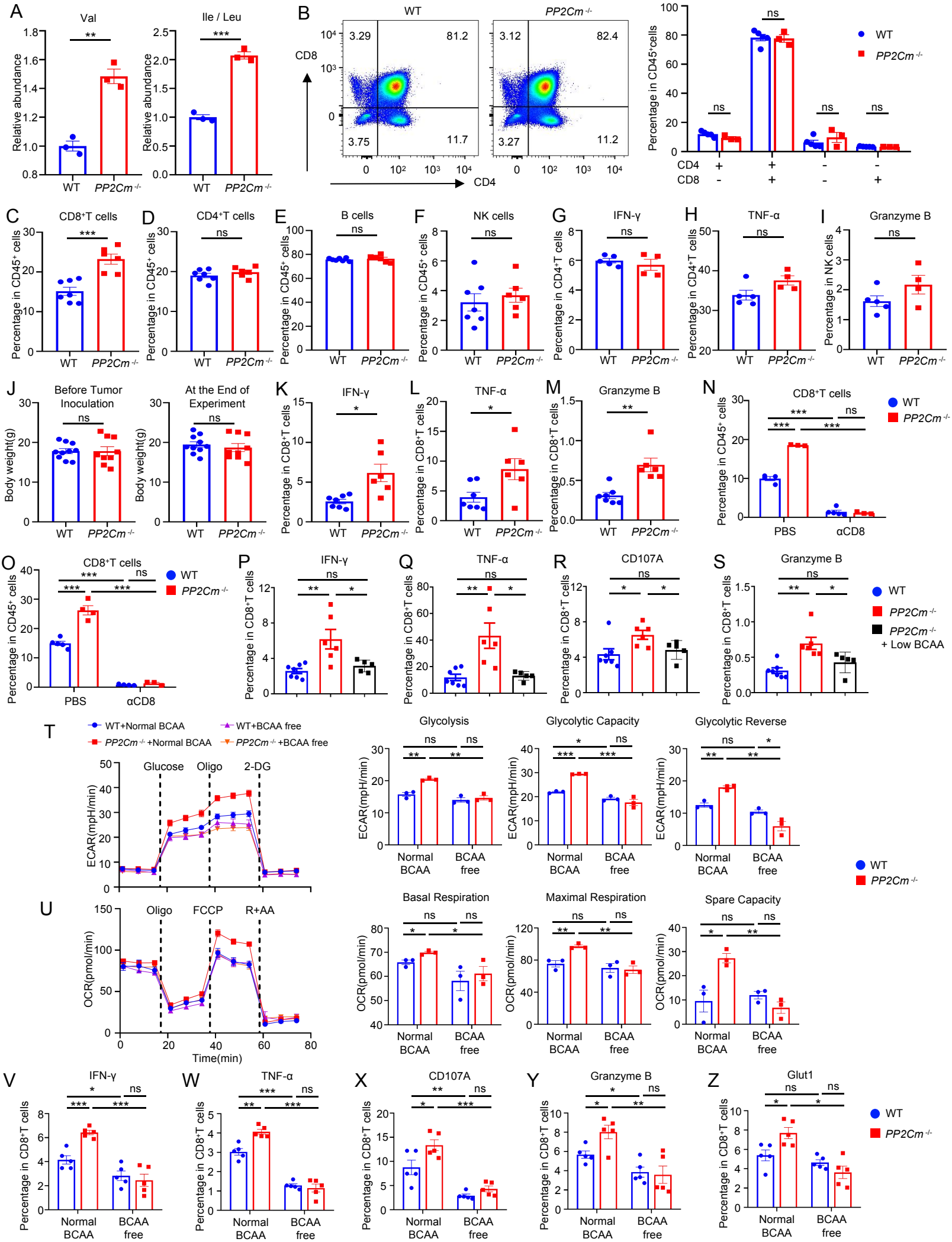
A
Val
Ile / Leu
Relative abundance
WT
PP2Cm -/-
B
WT
PP2Cm -/-
CD8
CD4
3.29
81.2
3.75
11.7
3.12
82.4
3.27
11.2
Percentage in CD45+cells
CD4
CD8
C
CD8+T cells
D
CD4+T cells
E
B cells
F
NK cells
G
IFN-γ
H
TNF-α
I
Granzyme B
Percentage in CD45+ cells
Percentage in CD4+T cells
Percentage in NK cells
J
Before Tumor Inoculation
At the End of Experiment
Body weight(g)
K
IFN-γ
L
TNF-α
M
Granzyme B
Percentage in CD8+T cells
N
CD8+T cells
PBS
αCD8
O
CD8+T cells
P
IFN-γ
Q
TNF-α
R
CD107A
S
Granzyme B
PP2Cm -/- + Low BCAA
T
WT+Normal BCAA
WT+BCAA free
PP2Cm -/- +Normal BCAA
PP2Cm -/- +BCAA free
Glucose
Oligo
2-DG
ECAR(mpH/min)
Glycolysis
Glycolytic Capacity
Glycolytic Reverse
Normal BCAA
BCAA free
U
Oligo
FCCP
R+AA
OCR(pmol/min)
Time(min)
Basal Respiration
Maximal Respiration
Spare Capacity
V
IFN-γ
W
TNF-α
X
CD107A
Y
Granzyme B
Z
Glut1

**Supplementary Figure 2. Related to Figure 1 — *PP2Cm*$^{-/-}$ mice exhibit enhanced CD8+ T cell functionality.**

(A) Comparisons of plasma levels of Val and Leu/Ile in WT (n = 3) versus *PP2Cm* $^{-/-}$ mice (n = 3) mice.

(B) Representative flow plots of the thymoctyes by CD4 and CD8 staining (left) and quantification of $CD4^+CD8^+$, $CD4^-CD8^-$, $CD4^+$ and $CD8^+$ thymocytes in the thymus (right) from WT (n = 5) versus *PP2Cm* $^{-/-}$ (n = 3) mice. Percentages in each quadrant were displayed.

(C-F) Frequencies of $CD8^+$ T cells (C), $CD4^+$ T cells (D), B cells (E) and NK cells (F) in the spleens of WT (n = 7) versus *PP2Cm* $^{-/-}$ mice (n = 6). Data from two independent experiments were pooled.

(G-I) Percentages of IFN-$\gamma^+$ (G), TNF-$\alpha^+$(H) of $CD4^+$ T cells and $GzmB^+$ (I) of NK cells in the spleens of WT (n = 5) versus *PP2Cm* $^{-/-}$ mice (n = 4).

(J) Body weight of WT (n = 10) versus *PP2Cm* $^{-/-}$ (n = 9) mice before tumor inoculation (left) and at the end of the experiments (right). Data from three independent experiments were pooled.

(K-M) Frequencies of IFN-$\gamma^+$ (K), TNF-$\alpha^+$ (L) and $GzmB^+$ (M) $CD8^+$ T cells in the spleens of WT (n = 7) versus *PP2Cm* $^{-/-}$ (n = 6) mice after bearing LLC tumors. Data from two independent experiments were pooled.

(N) Frequencies of $CD8^+$ T cells in the spleens of LLC tumor mouse model after anti-CD8 antibody treatment in WT (n = 4), *PP2Cm* $^{-/-}$ (n = 3), WT+anti-CD8 (n = 5) and *PP2Cm* $^{-/-}$+anti-CD8 (n = 3) mice.

(O) Frequencies of $CD8^+$ T cells in the spleens of B16-F10 tumor mouse model after anti-CD8 antibody treatment in WT (n = 5), *PP2Cm* $^{-/-}$ (n = 4), WT+anti-CD8 (n = 4) and *PP2Cm* $^{-/-}$+anti-CD8 (n = 3) mice.

(P-S) Percentages of IFN-$\gamma^+$ (P), TNF-$\alpha^+$ (Q), $CD107A^+$ (R) and $GzmB^+$ (S) $CD8^+$ T cells in *PP2Cm* $^{-/-}$ mice fed with normal diet (n = 6) and with BCAA-low diet (n = 5).

(T) ECAR influxes of $CD8^+$ T cells from WT (n = 3) versus *PP2Cm* $^{-/-}$ mice (n = 3) activated in culture media containing normal BCAA and no BCAA.

(U) OCR influxes of $CD8^+$ T cells from WT (n = 3) versus *PP2Cm* $^{-/-}$ mice (n = 3) activated in culture media containing normal BCAA and no BCAA.

(V-Z) Percentages of IFN-$\gamma^+$ (V), TNF-$\alpha^+$ (W), $CD107A^+$ (X), $GzmB^+$ (Y) and $Glut1^+$ (Z) $CD8^+$ T cells from WT (n = 5) versus *PP2Cm* $^{-/-}$ mice (n = 5) upon anti-CD3/CD28 stimulation in culture media containing normal BCAA and no BCAA with.

Data are presented as mean ± SEM. ns: non-significant, *p < 0.05, **p < 0.01, ***p < 0.001 by the *Student's t* test (A-Z). Unless indicated, data were the representative of two independent experiments.

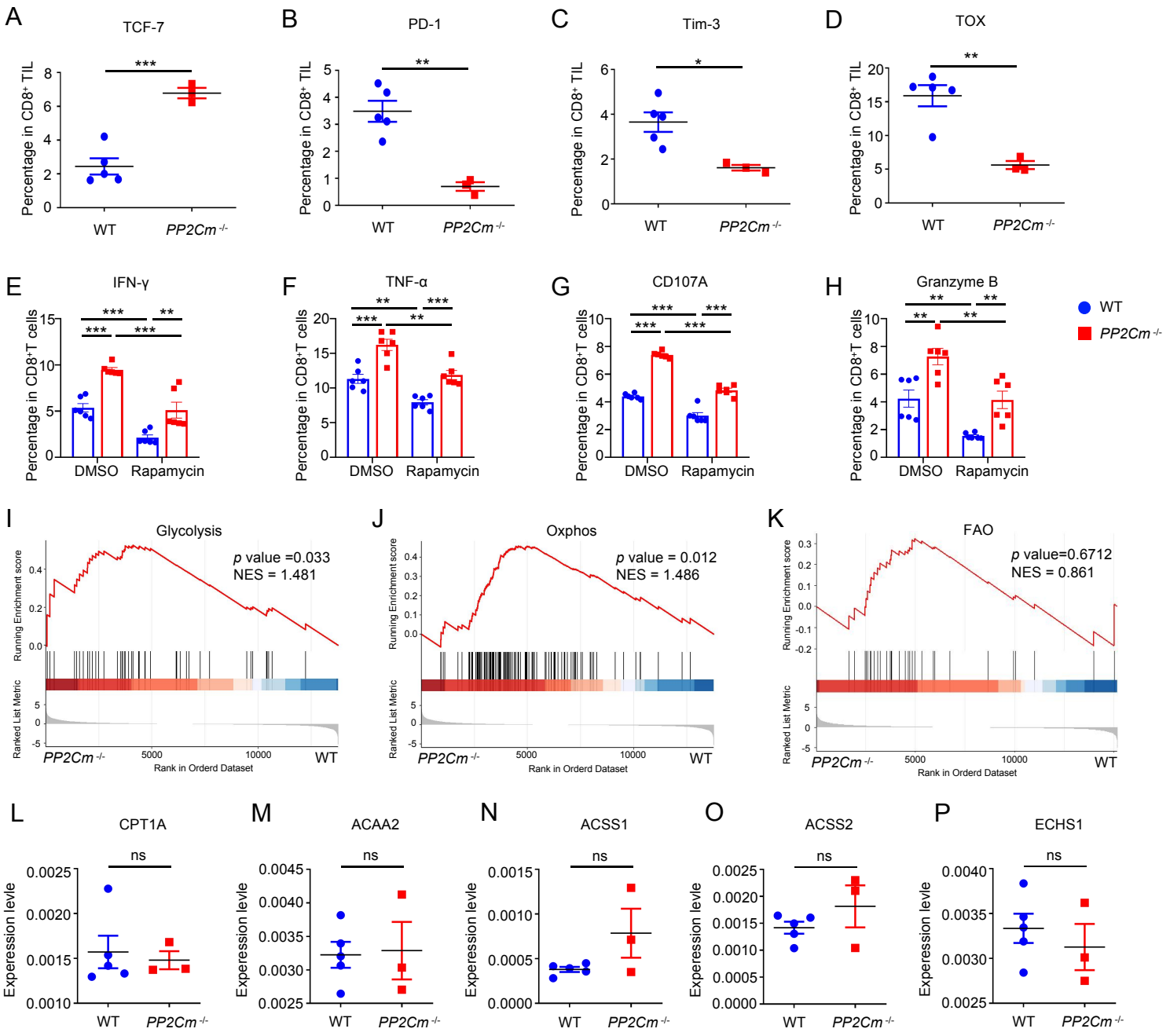


**Supplementary Figure 3. Related to Figure 2 and 3 — CD8⁺ T cells from *PP2Cm*$^{-/-}$ mice exhibit less exhausted phenotypes with altered metabolic features.**

(A-D) Percentages of TCF-7⁺ (A), PD-1⁺ (B), Tim-3⁺ (C) and TOX⁺ (D) CD8⁺ T cells infiltrated in LLC tumors from WT (n = 5) versus *PP2Cm* $^{-/-}$ (n = 3) mice.

(E-H) Percentages of IFN-γ⁺ (E), TNF-α⁺ (F), CD107A⁺ (G), GzmB⁺ (H) CD8⁺ T cells from WT (n = 6) versus *PP2Cm* $^{-/-}$ (n = 6) mice upon treatment with Rapamycin versus DMSO.

(I-K) GSEA analysis indicating gene sets involved in glycolysis (I), OXPHOS (J) and fat acid oxidation (FAO) metabolism (K) in CD8⁺T cells from *PP2Cm* $^{-/-}$ versus WT mice.

(L-P) Comparisons of *CPT1A* (L), *ACAA2* (M), *ACSS1* (N), *ACSS2* (O), *ECHS1* (P) expressions related to FAO in CD8⁺ T cells from WT (n = 5) versus *PP2Cm* $^{-/-}$ (n = 3) mice by qPCR.

Data are presented as mean ± SEM. ns: non-significant, *p < 0.05, **p < 0.01, ***p < 0.001 by the *Student's t* test (A-H, L-P). Data were representative of two independent experiments.

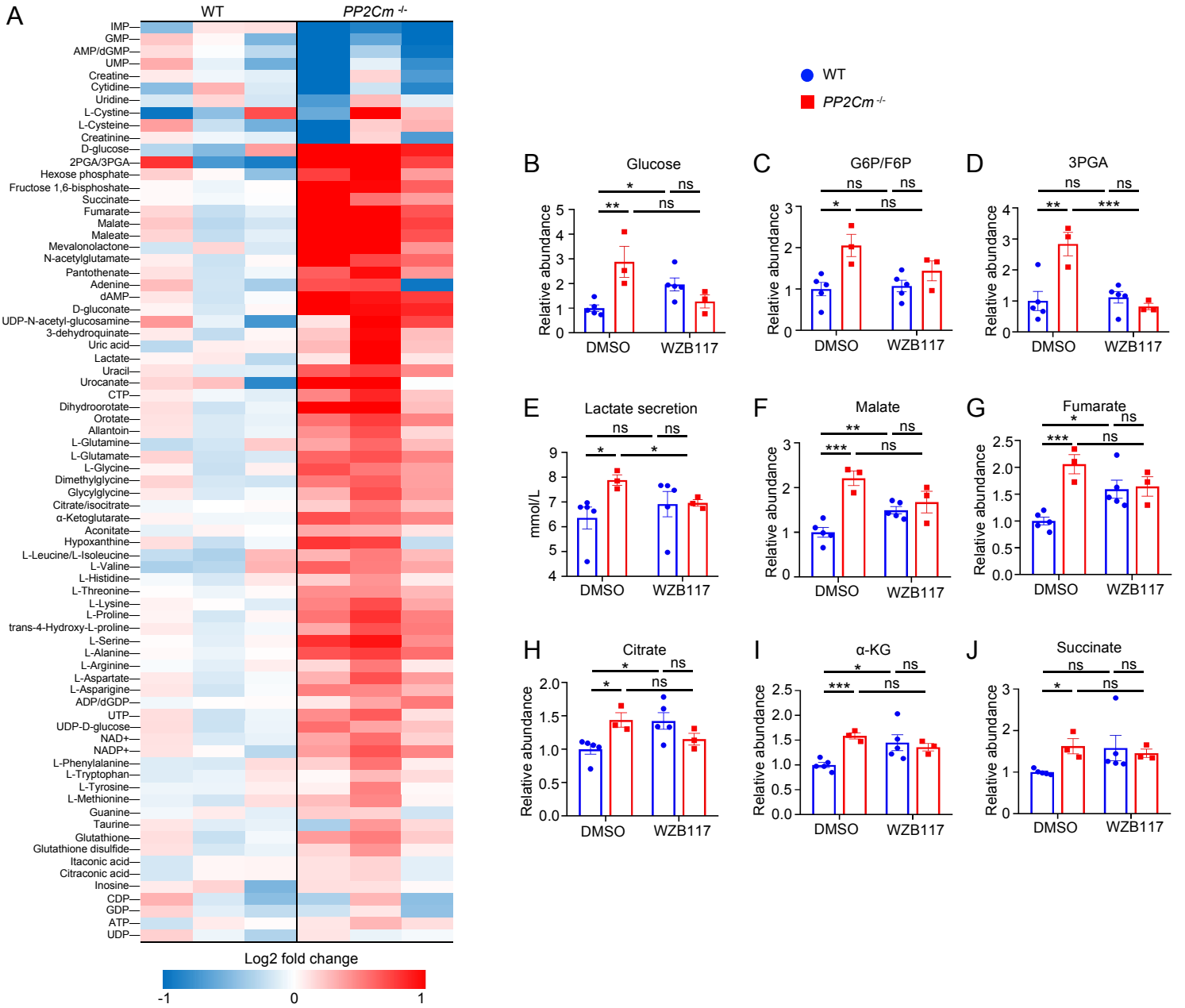


**Supplementary Figure 4. Related to Figure 3 — *PP2Cm* deficiency in CD8⁺ T cells promotes glycolysis and OXPHOS activities in a Glut1 dependent manner.**

(A) Heatmaps of intracellular metabolites in WT (n = 3) versus *PP2Cm* $^{-/-}$ (n = 3) CD8⁺ T cells.

(B-J) Intermediate metabolites related to glucose consumption in anti-CD3/CD28 activated CD8⁺ T cells from WT (n = 5) versus *PP2Cm*$^{-/-}$ (n = 3) mice upon treatment with DMSO or WZB117.

Data are presented as mean ± SEM. *p < 0.05, **p < 0.01, ***p < 0.001 by the *Student's t* test (B-J). Data were representative of two independent experiments.

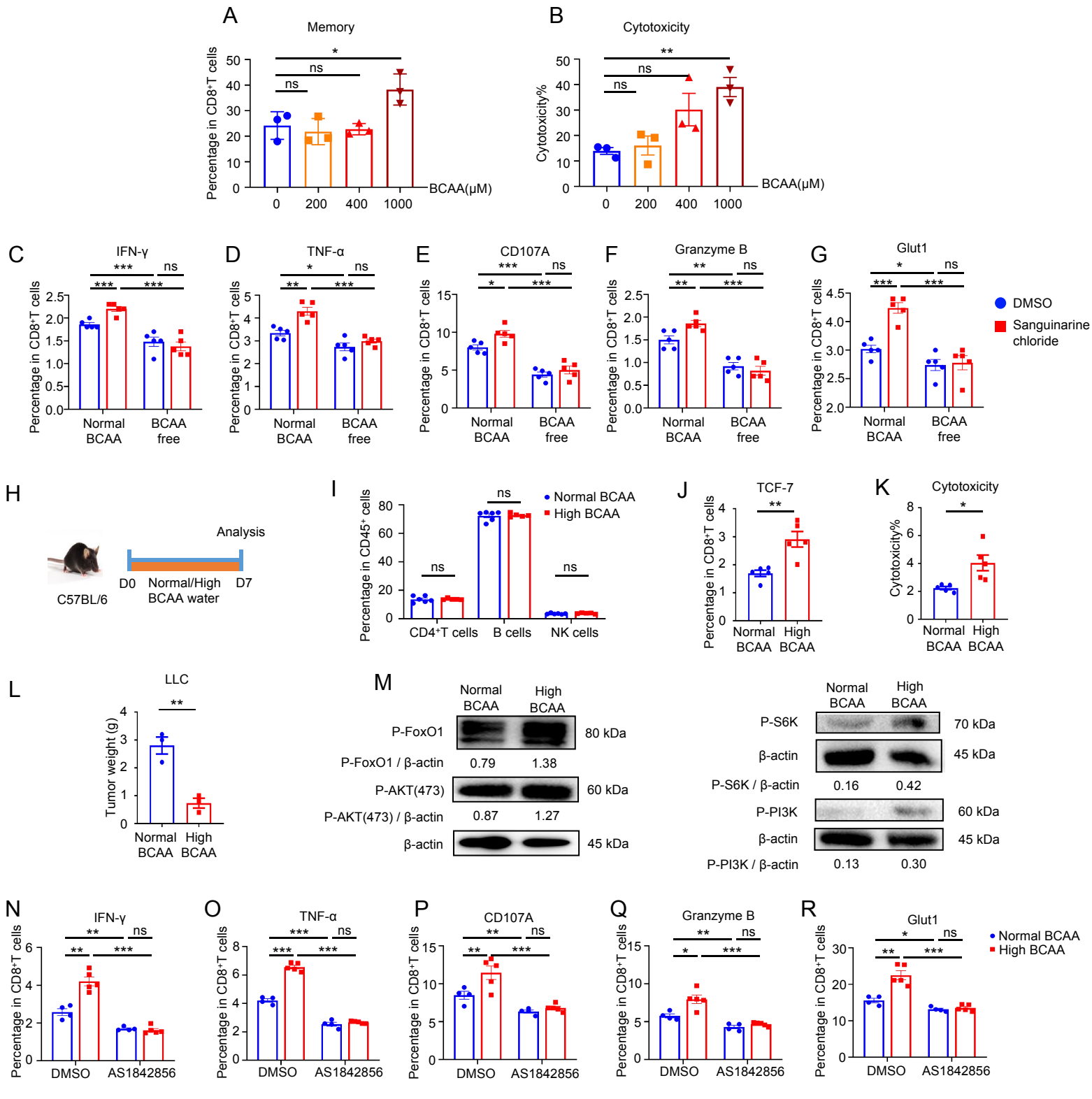
A
Memory
Percentage in CD8+T cells
BCAA(μM)
B
Cytotoxicity
Cytotoxicity%
C
IFN-γ
D
TNF-α
E
CD107A
F
Granzyme B
G
Glut1
Normal BCAA
BCAA free
DMSO
Sanguinarine chloride
H
C57BL/6
Analysis
D0
Normal/High BCAA water
D7
I
Normal BCAA
High BCAA
CD4+T cells
B cells
NK cells
J
TCF-7
K
Cytotoxicity
L
LLC
Tumor weight (g)
M
P-FoxO1
80 kDa
P-FoxO1 / β-actin
0.79
1.38
P-AKT(473)
60 kDa
P-AKT(473) / β-actin
0.87
1.27
β-actin
45 kDa
P-S6K
70 kDa
P-S6K / β-actin
0.16
0.42
P-PI3K
60 kDa
P-PI3K / β-actin
0.13
0.30
N
IFN-γ
O
TNF-α
P
CD107A
Q
Granzyme B
R
Glut1
DMSO
AS1842856

**Supplementary Figure 5. Related to Figure 4 — BCAA supplementation enhances $CD8^+$ T cells functionality with hyper-activation of mTOR-PI3K-AKT-FoxO1 signaling axis.**

(A) Percentages of WT memory $CD8^+$ T cells upon anti-CD3/28 stimulation for 24 h with BCAAs at gradient concentrations. (n = 3)

(B) Killing activities of $CD8^+$ T cells to LLC cells after anti-CD3/28 stimulation for 24 h with BCAAs at gradient concentrations by LDH release assay. (n = 3)

(C-G) Percentages of IFN-$\gamma^+$ (C), TNF-$\alpha^+$ (D), $CD107A^+$ (E), $GzmB^+$ (F) and $Glut1^+$ (G) $CD8^+$ T cells from WT mice (n = 5) upon anti-CD3/CD28 stimulation in culture media containing normal and no BCAAs with or without PP2Cm inhibitor Sanguinarine chloride.

(H) Experimental scheme.

(I) Frequencies of $CD4^+$ T cells, B cells and NK cells in the spleens of normal (n = 5) versus high BCAAs (n = 5) fed mice.

(J) Frequencies of TCF-$7^+$ $CD8^+$T cells in the spleens of normal (n = 5) versus high BCAAs (n = 5) fed mice.

(K) Killing activities of $CD8^+$ T cells upon anti-CD3/28 stimulation of normal (n = 5) versus high BCAAs (n = 5) fed mice to LLC cells by LDH release assay.

(L) LLC tumor growth in *Rag*$^{-/-}$ mice adoptively transferred with $CD8^+$ T cells from normal (n = 3) and high (n = 3) BCAA-fed mice.

(M) Immunoblotting analysis of the indicated proteins in $CD8^+$ T cells from normal versus high BCAAs fed mice upon anti-CD3/28 stimulation for 30 min.

(N-R) Percentages of IFN-$\gamma^+$ (N), TNF-$\alpha^+$ (O), $CD107A^+$ (P), $GzmB^+$ (Q) and $Glut1^+$(R) $CD8^+$ T cells from normal (n = 4) versus high BCAAs (n = 5) fed mice after anti-CD3/28 stimulation with DMSO or AS1842856 for 72 h.

Data are presented as mean ± SEM. ns: non-significant, *p < 0.05, **p < 0.01, ***p < 0.001 by the *Student's t* test (A-R). Data were representative of two independent experiments.

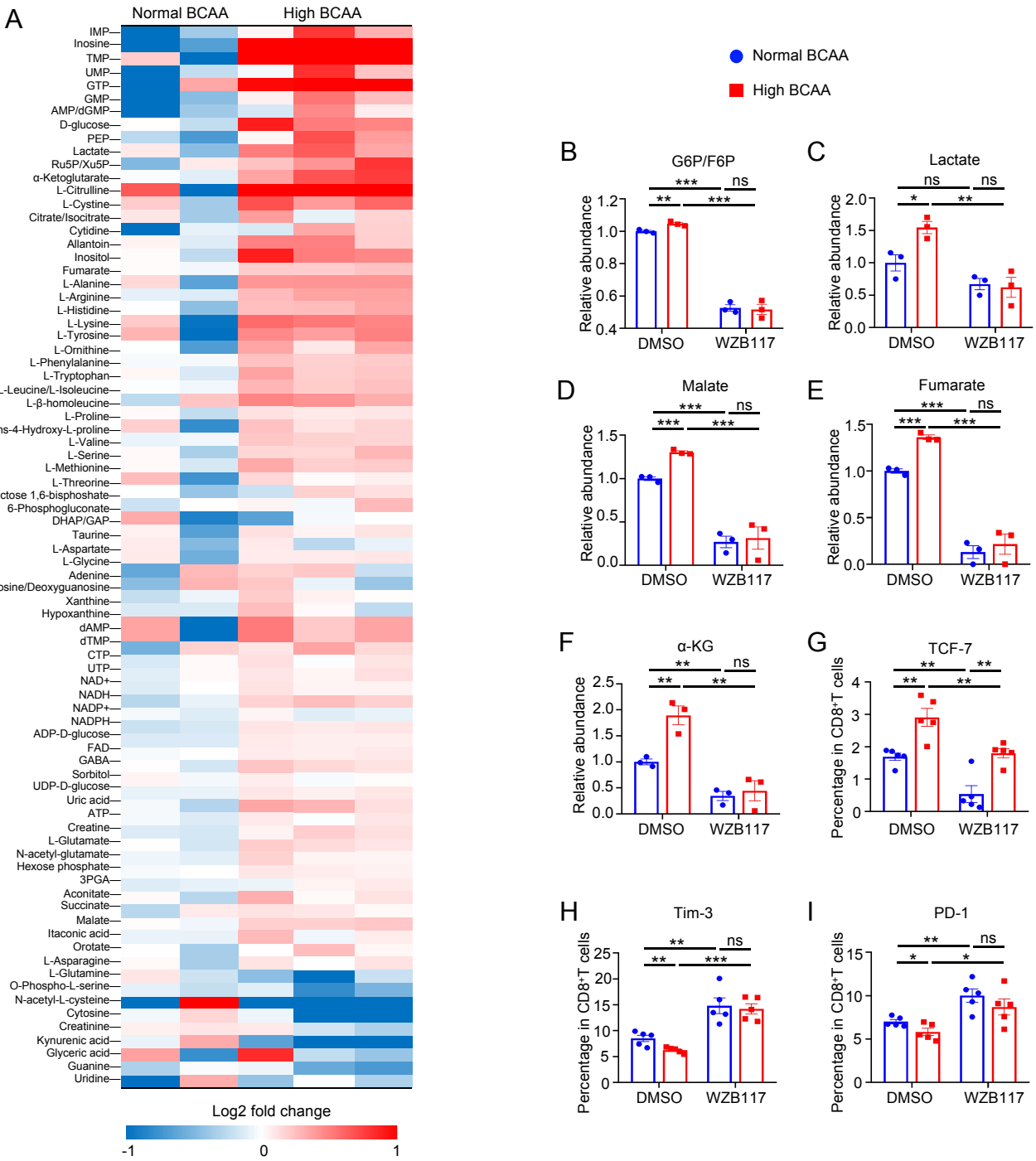


**Supplementary Figure 6. Related to Figure 4 — BCAA supplementation in CD8⁺ T cells promotes glycolysis and OXPHOS activities in a Glut1 dependent manner.**

(A) Heatmaps of intracellular metabolites in CD8⁺ T cells from normal (n = 2) versus high BCAAs (n = 3) fed mice.

(B-F) Intracellular metabolites related to glycolysis including G6P/F6P (B), lactate (C), and the TCA-cycle activity including malate (D), fumarate (E) and a-KG (F) in CD8⁺ T cells from normal (n = 3) versus high BCAAs (n = 3) fed mice upon anti-CD3/28 stimulation with DMSO or WZB117 treatment for 24 h.

(G-I) Percentages of TCF-7⁺ (G), Tim-3⁺ (H) and PD-1⁺ (I) CD8⁺ T cells from normal (n = 4) versus high BCAA (n = 5) fed mice upon anti-CD3/28 stimulation with DMSO or WZB117 for 72 h.

Data are presented as mean ± SEM. ns: non-significant, *p < 0.05, **p < 0.01, ***p < 0.001 by the *Student's* t test (B-I). Data were representative of two independent experiments.

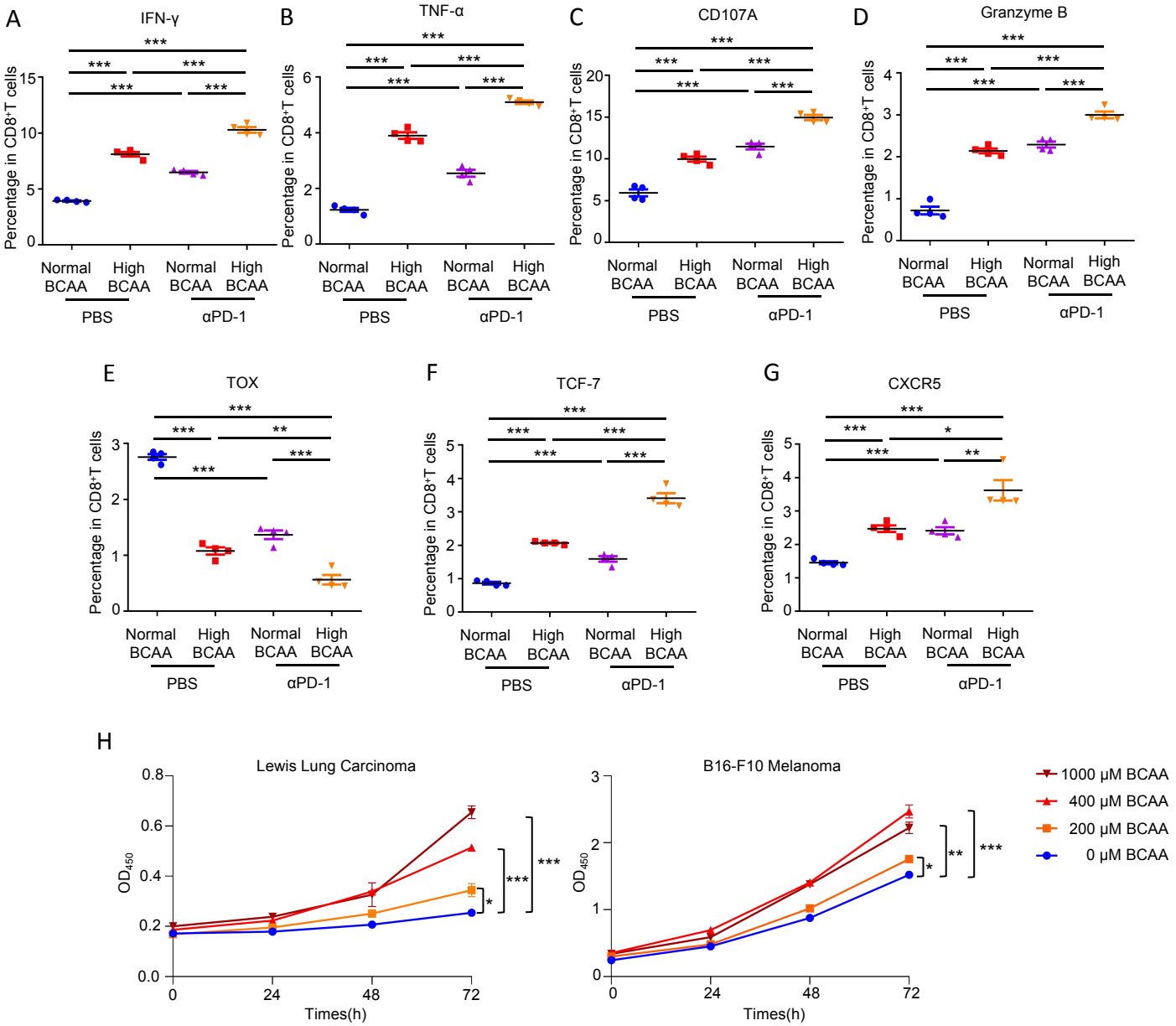


**Supplementary Figure 7. Related to Figure 5 — BCAA supplementation synergizes with anti-PD-1 treatment to promote anti-tumor immunity.**

(A-G) Percentages of IFN-γ$^+$ (A), TNF-α$^+$ (B), CD107A$^+$ (C), GzmB$^+$ (D), TOX$^+$ (E), TCF-7$^+$ (F) and CXCR5$^+$ (G) CD8$^+$ T cells from normal (n = 4) versus high BCAAs (n = 4) fed mice with or without anti-PD-1 treatment in B16-F10 tumor-bearing mice.

(H) *In vitro* proliferation curves of LLC (left) and B16-F10 (Right) cells with gradient BCAA concentrations by CCK-8 assays.

Data are presented as mean ± SEM. ns: not-significant, *p < 0.05, **p < 0.01, ***p < 0.001 by the *Student's t* test (A-H). Data were representative of two independent experiments.

**Supplementary Table1 — Clinical manifestations of advanced NSCLC patients receiving nivolumab treatment with different responses**

| Characteristics | | R (n=10) | NR (n=14) | *p*value |
|---|---|---|---|---|
| Age | | 61.90 ± 3.20 | 58.71 ± 2.72 | 0.457 |
| Tumor diameter（mm） | | 55.89 ± 9.52 | 54.01 ± 7.48 | 0.876 |
| ANC（$10^9$/L） | | 4.50 ± 0.45 | 4.83 ± 0.48 | 0.637 |
| BPC ($10^9$/L) | | 217.50 ± 16.18 | 258.00 ± 17.46 | 0.117 |
| ALC ($10^9$/L) | | 1.43 ± 0.12 | 1.36 ± 0.11 | 0.669 |
| LDH (U/L) | | 204.78 ± 19.50 | 262.30 ± 26.64 | 0.126 |
| Gender | Male/Female | 2/8 | 6/8 | 0.252 |
| Smoke | Non-smoker/smoker | 4/6 | 7/7 | 0.635 |
| Type | SquamousAdenocarcinomaLarge-Cell-Neuroendocrine | 370 | 2111 | 0.261 |

R: responders, NR: non-responders, ANC: absolute neutrophil Count, BPC: blood platelets count, ALC: absolute lymphocyte count, LDH: lactate dehydrogenase.